2020

Geologic Characterization, Hydrologic Monitoring, and Soil-Water Relationships for Landslides in Kentucky

Matthew M. Crawford
University of Kentucky, mcrawford@uky.edu

L. Sebastian Bryson
University of Kentucky, sebastian.bryson@uky.edu

Zhenming Wang
University of Kentucky, zhenming.wang@uky.edu

Edward W. Woolery
University of Kentucky, ewoolery@uky.edu

Kentucky Geological Survey
William C. Haneberg, State Geologist and Director
University of Kentucky, Lexington

Geologic Characterization, Hydrologic Monitoring, and Soil-Water Relationships for Landslides in Kentucky

Matthew M. Crawford, L. Sebastian Bryson, Zhenming Wang, and Edward W. Woolery

Report of Investigations 11 doi.org/10.13023/kgs.ri11.13 Series XIII, 2020

Our Mission

The Kentucky Geological Survey is a state-supported research center and public resource within the University of Kentucky. Our mission is to support sustainable prosperity of the commonwealth, the vitality of its flagship university, and the welfare of its people. We do this by conducting research and providing unbiased information about geologic resources, environmental issues, and natural hazards affecting Kentucky.

Earth Resources—Our Common Wealth

www.uky.edu/kgs

Technical Level

General Intermediate Technical

Statement of Benefit to Kentucky

Hillslope soil moisture is one of many important factors that influence landslide occurrence. Field investigations that monitor soil moisture, rainfall, soil-water relationships, and landslide movement can contribute to a better understanding of conditions that lead to landslides. This report summarizes field techniques and research methodology to connect soil properties, soil mechanics, and geology, and serves as a sound scientific basis for broad landslide hazard characterization, as well as future slope-stability assessments.

ISSN 0075-5591

Contents

Abstract....1
Introduction....1
Study Sites....2
Roberts Bend....2
Doe Run....3
Herron Hill....4
Methodology....6
Soil-Moisture Sensors....6
Rain Gage....8
Data Collection and Power Supply....9
Observations....11
Rainfall and Landslide Activity....11
Soil Moisture....13
Soil-Water Relationships....13
Field Soil-Water Characteristic Curves....13
Modeled Soil-Water Characteristic Curves....14
Relationship With and Implications for Shear Strength....16
Suction Stress....22
Summary....22
Acknowledgments....24
References Cited....25

Figures

1. Combined hillshade map and aerial photograph of the Roberts Bend landslide complex....3
2. Combined hillshade map and aerial photograph of the Doe Run landslide complex....5
3. Combined hillshade map and aerial photograph of the Herron Hill landslide complex....7
4. Photographs of soil pits, sensor locations, and soil interpretation at the Doe Run, Roberts Bend, and Herron Hill landslides....9
5. Graph showing volumetric water response to rainfall on June 18, 2015, from 7 to 11 p.m. at the Doe Run landslide....10
6. Photograph of a field station at the Roberts Bend landslide....11
7. Graph showing average cumulative rainfall and documented landslides in Kentucky....12
8. Graph showing cumulative horizontal displacement measured by cable extension transducer and rainfall at the Roberts Bend landslide....12
9. Graph showing volumetric water content and horizontal displacement during a transition from dry through a wetting phase, toward near-saturated conditions, in late 2016 at the Roberts Bend landslide....13
10. Graph showing cumulative rainfall at the Roberts Bend landslide from late October 2015 to late April 2019....14
11. Graph showing volumetric water content below the U.S. Forest Service road at the Roberts Bend landslide....14
12. Graph showing volumetric water content above the U.S. Forest Service road at the Roberts Bend landslide....15
13. Graph showing water potential below the U.S. Forest Service road at the Roberts Bend landslide....15

Figures (continued)

14. Graph showing water potential above the U.S. Forest Service road at the Roberts Bend landslide 16
15. Graph showing cumulative rainfall at the Doe Run landslide from early May 2015 to early March 2019 16
16. Graph showing volumetric water content, upslope and downslope, at the Doe Run landslide 17
17. Graph showing water potential, upslope and downslope, at the Doe Run landslide 17
18. Graph showing cumulative rainfall at the Herron Hill landslide from mid-September 2015 to mid-May 2017 18
19. Graph showing volumetric water content, upslope and downslope, at the Herron Hill landslide 18
20. Graph showing water potential, upslope and downslope, at the Herron Hill landslide 19
21. Graph showing typical soil-water characteristic curves for sandy, silty, and clayey soils 19
22. Graphs showing field soil-water characteristic curves for (a) the Doe Run landslide upslope at a depth of 70 cm and (b) the Herron Hill landslide upslope at a depth of 90 cm 20
23. Graphs showing soil-water characteristic curve for soil downslope at 44 cm depth at the Roberts Bend landslide (a) and the modeled curve using the drying path (b) 20
24. Graphs showing shear strength and water potential for all three landslides at various locations and depths 21
25. Graphs showing suction stress as a function of electrical conductivity at two locations at the Roberts Bend landslide 23

Tables

1. Field descriptions of colluvial soil at the Roberts Bend landslide 4
2. Soil properties at selected soil pits at the Roberts Bend landslide 4
3. Field descriptions of colluvial soil at the Doe Run landslide 6
4. Soil properties at selected soil pits in the Doe Run landslide 6
5. Field descriptions of colluvium and weathered bedrock at the Herron Hill landslide 8
6. Soil properties at selected pits in the Herron Hill landslide 8
7. Volumetric water-content specifications 9
8. Water-potential sensor specifications 9
9. Slope locations, sensor types, and depth at all landslides 10
10. Data tables and parameters collected at each landslide 11
11. Statewide average cumulative rainfall across Kentucky 11
12. Shear-strength and volumetric-water-content parameters used in equation 7 20

Geologic Characterization, Hydrologic Monitoring, and Soil-Water Relationships for Landslides in Kentucky

Matthew M. Crawford, L. Sebastian Bryson, Zhenming Wang, and Edward W. Woolery

Abstract

Complex spatial and temporal variables control the movement of water through colluvial soils in hillslopes. Some of the factors that influence soil-moisture fluctuation are soil type, thickness, porosity and permeability, and slope morphology. Landslide-characterization and field-monitoring techniques were part of a method to connect hydrologic and geotechnical data in order to monitor long-term hydrologic conditions in three active landslides in Kentucky, establish hydrologic relationships across the slope, and analyze specific soil-water relationships that can predict shear strength. Volumetric water content, water potential, and electrical conductivity were measured between October 2015 and February 2019. The duration and magnitude of drying and wetting within the soil varied for each slope location and soil depth, suggesting that differences in slope morphology, soil texture, and porosity influence the water-infiltration process, as well as shear strength and general landslide dynamics. The parameters measured and soil-water relationships were also compared to rainfall and slope movement at one of the landslides.

The method used to acquire hydrologic data was cost-effective, and the field techniques may be useful for subsequent projects, such as slope-stability assessments and landslide-susceptibility modeling. Hydrologic parameters, volumetric water content, and water potential are pertinent to investigating the stability of landslides, which are often triggered or reactivated by rainfall. These methods can be used to support landslide-hazard assessment and improve our understanding of the long-term influence of moisture conditions in hillslope soils.

Introduction

Landslides occur when the shear stresses imposed on a slope exceed the slope's available shear strength—i.e., when resisting forces such as friction and cohesion are overcome by a stress load. These stresses can include increased pore-water pressure (from rainfall), gravity, or some type of slope modification, such as loading or excavating during construction.

Landslides in Kentucky are primarily triggered by rainfall and occur in shallow colluvial soils. Colluvial soils cover hillslopes and are typically poorly sorted, with grain sizes that range from clay size to large rock fragments perhaps a meter or more in width (Turner, 1996). Landslides in colluvial soils are commonly either thin (less than 2 m thick) translational slides or thicker rotational slumps, and both types of landslides are capable of morphing into damaging debris flows

or debris slides, especially on steep slopes (Fleming and Johnson, 1994; Cruden and Varnes, 1996; Turner, 1996). Landslide behavior and stability, especially for shallow colluvial landslides, are highly influenced by fluctuating water content and stresses in the unsaturated zone (Godt and others, 2009, 2012; Bittelli and others, 2012; Lu and Godt, 2013). Stresses in the unsaturated zone vary because of transient water flow, perched water, and various soil properties.

In-situ soil systems are partially saturated and exhibit fluctuations in matric suction (water potential), which is the difference between the pore-air pressure and the pore-water pressure. Water potential and effective stress are reduced by rainfall, increasing the likelihood of landslides (Godt and others, 2009; Lu and Godt, 2013; Oh and Lu, 2015).

We monitored three landslides in Kentucky between October 2015 and February 2019. The site descriptions, field methodology, data-acquisition techniques, and observations resulting from this monitoring provide a general picture of soil moisture in hillslope soils. Rainfall, volumetric water content, water potential, electrical conductivity, effective saturation, and suction stress were either directly measured or determined from in-situ measurements. Reports by Baum and others (2010) and Smith and others (2013) helped guide the methods for hydrologic monitoring.

The field techniques and methodology developed in this study for data acquisition and evaluation may be useful to other field monitoring projects or landslide-hazard assessments. The field instrumentation and implementation described in this report are cost-effective techniques that can be used for subsequent projects such as slope-stability assessment and landslide-susceptibility modeling.

This report is part of an extensive project that developed a methodology and site-specific framework, using field and laboratory techniques, to correlate soil-water relationships, in-situ electrical data, and surface electrical tomography in order to assess soil shear strength. For additional detail on the project, see Crawford (2018); raw data for the project are archived at the Kentucky Geological Survey and are available upon request.

Study Sites

Roberts Bend

The Roberts Bend landslide in Pulaski County, near Burnside, Ky., is along the western edge of the Appalachian Plateau. The study area is on a variably steep, forested slope adjacent to a sharp meander in the South Fork of the Cumberland River (Fig. 1). The underlying bedrock is light greenish gray to reddish brown clay-shale with interbeds of sandstone, limestone, and minor dolomite and siltstone. Throughout the Appalachian Plateau, the distinct hummocky topography that forms on the shale is susceptible to landslides, especially when wet (Taylor and others, 1975). The slope angle at this landslide, between ridgetop and midslope, ranges from approximately 18 to 25°. The lowermost part of the slope is very steep with near-vertical cliffs that reach down to the river. The local relief between the river and the ridgetop is about 145 m. Several flat topographic benches can be traced along contour and are indicators of changes in bedrock lithology. These topographic benches are bedrock controlled, but also influence the movement of surficial deposits along the hillslopes. A U.S. Forest Service road crosses the slope, separating distinct landslide morphologies.

The landslide is a complex of shallow and possibly deep-seated landslides of various relative ages. The morphology of the landslide complex varies above and below the Forest Service road. Upslope of the road, landslide features are somewhat subdued, except for a prominent headscarp that defines the upper extent of the landslide area. Below the road, there are several recent, nested landslides that have well-defined scarps, distinct flank features, hummocks, and toe bulges. Rotation in the head of this area below the Forest Service road is evident from back-tilting of trees and the ground surface. Electrical-resistivity surveys indicate variable depths of interpreted failure zones, ranging from 1 m upslope to approximately 4 m downslope where there is hummocky, rotational landslide activity (Crawford and others, 2018).

In order to describe the colluvium at Roberts Bend (Table 1), we dug three pits by hand (indicated by the blue dots in Figure 1): two above the road and one below. Soil-classification parameters are listed in Table 2. Natural gravimetric water contents and Atterberg limits were determined ac-

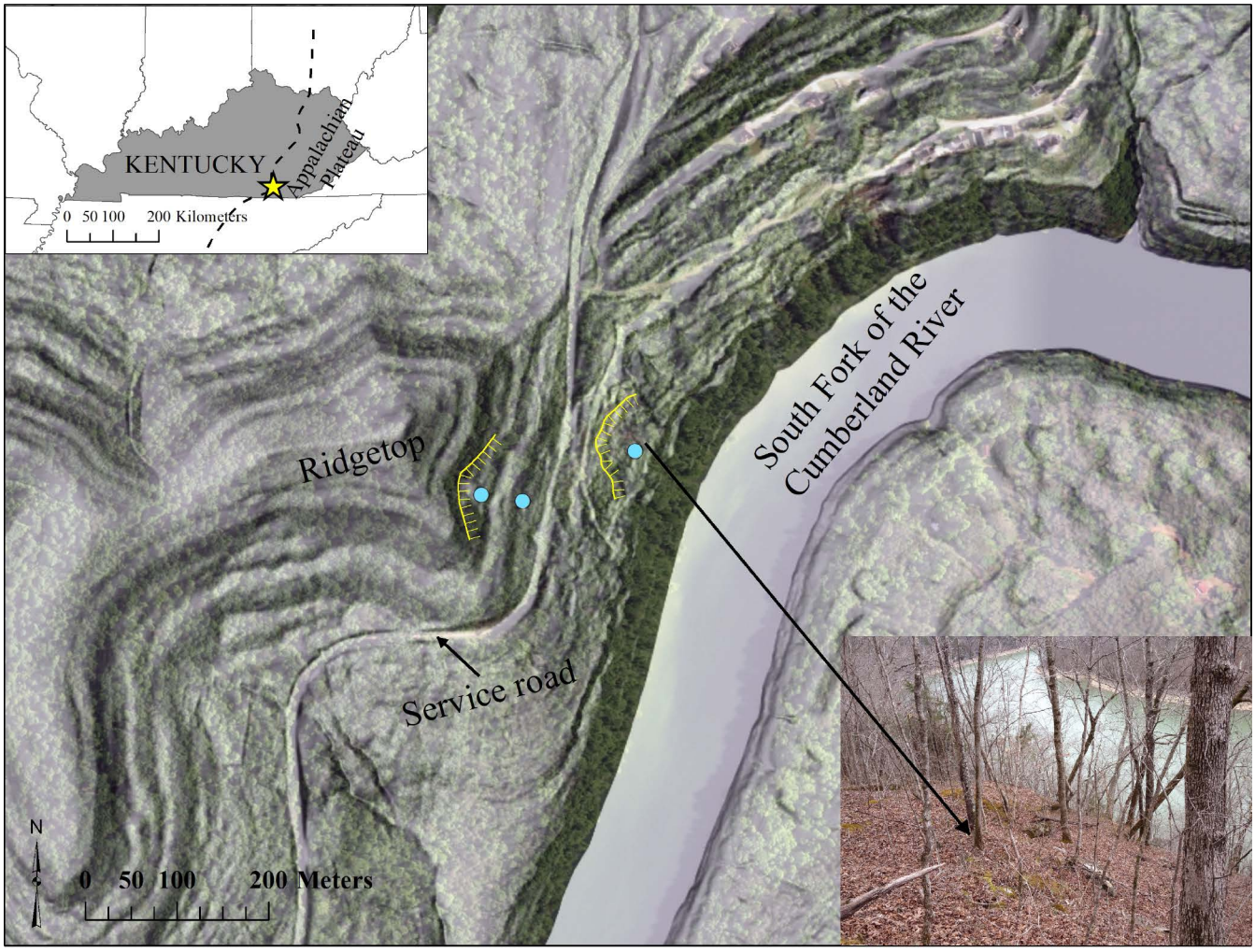

Figure 1. Combined hillshade and aerial photograph of the Roberts Bend landslide complex. The blue dots indicate the soil-monitoring locations along the slope. Yellow lines indicate landslide scarps. The dashed line on the index map indicates the western boundary of the Appalachian Plateau. The yellow star on the index map indicates the general location of the site. The inset photo is of a downslope nested landslide near a steep drop toward the river.

cording to ASTM standards D2216 and D4318, respectively. The Unified Soil Classification System designations were determined according to the Natural Resources Conservation Service soils data for Kentucky.

Doe Run

The Doe Run landslide in Kenton County, near Erlanger, is in northern Kentucky, just south of Cincinnati, Ohio, in the Outer Bluegrass physiographic region. Landslides are prevalent in northern Kentucky, damaging roads, commercial property, and private residences. As suburban development increases, infrastructure has invaded more steep hillsides, increasing their susceptibility to failure (Fleming and Johnson, 1994; Crawford, 2012). The landslide is in Doe Run Lake Park, along the outside meander of Bullock Pen Creek, which flows into a reservoir (Fig. 2). This site was chosen because (1) it is an active landslide on an unmodified slope with easy access for setting up field instruments and equipment, (2) it is representative of typical landslides in the area, and (3) local government authorities granted us permission to work in the park. The area is characterized by steep slopes, incised valleys, shaly bedrock, and weak colluvial soils (Fleming and Johnson, 1994; Potter, 2007). The Natural Resources Conservation Service identifies the soil at Doe Run as an Eden silty clay loam (kygeonet.ky.gov/kysoils). The bedrock formation underlying the landslide is the Ordovician

Table 1. Field descriptions of colluvial soil at the Roberts Bend landslide	
Above Road Pit, Upslope (Depth, cm)	*Soil Description*
0–10	Dark brown topsoil, organic-rich.
10–20	Silty clay, brown.
20–45	Silty clay, light brown, few rock fragments.
45–75	Gray to bluish clay-shale, soft, slightly fissile, few rock fragments.
75–79	Red clay-shale, stiff, weathered.
95–100	Weathered shale.
Above Road Pit, Midslope (Depth, cm)	*Soil Description*
0–5	Dark brown topsoil, organic rich.
5–30	Reddish brown, silty clay, soft.
30–45	Dark red, clayey to silty shale, stiff, few rock fragments.
45–75	Brownish gray to red, silty clay-shale, mottled, few rock fragments.
75–95	Grayish green to brown, silty to sandy clay-shale, weathered, abundant rock fragments.
Above Road Pit, Downslope (Depth, cm)	*Soil Description*
0–13	Light to dark brown, silty clay.
13–44	Light brown to gray, clayey soil, soft, blocky, few rock fragments.
44–75	Light gray to greenish gray clay-shale, mottled, sandy streaks.

Kope Formation, which consists of 75 to 80 percent shale and 20 to 25 percent interbedded limestone. Limestone content increases upslope toward a more resistant Fairview Formation. Because of the Kope's soft, deformable shale, the formation weathers and erodes easily, often slumping when wet (Luft, 1969). The colluvium varies in thickness depending on slope angle and morphology. Between the toe slope and midslope, the thickness can reach 15 m and can thin to a meter or less between the midslopes toward ridgetops. The slope angle ranges from approximately 21° midslope to approximately 12° at the toe.

The extent of the slide is difficult to discern, because the entire ridge can be classified as a large landslide complex. Headscarps and landslide flanks are also difficult to observe, except for a small slump at the toe of the slope. The length of the downslope axis of the monitored slide area is approximately 52 m. Approximately 120 m downstream from the monitored site is a thin, translational landslide that occurred in the fall of 2011. Its failure surface is interpreted to be along the colluvium-bedrock interface. The headscarp height was approximately 1 m and the slide length measured approximately 46 m. This landslide destroyed a hiking trail and partially dammed the creek.

Doe Run is an excellent monitoring site because it is in an area known for landslides, landslide features can be readily observed, and it is near another recent damaging landslide.

To describe and classify the landslide, we dug two pits by hand (blue dots in Figure 2): one upslope and one downslope near the toe. Field soil descriptions and index properties are listed in Tables 3 and 4, respectively. Natural gravimetric water contents and Atterberg limits were determined according to ASTM standards D2216 and D4318, respectively. The Unified Soil Classification System designations were determined according to the Natural Resources Conservation Service soils data for Kentucky.

Table 2. Soil properties at selected soil pits at the Roberts Bend landslide.					
Location	*Depth (cm)*	*Natural Gravimetric Water Content (%)*	*Liquid Limit (%)*	*Plasticity Index (%)*	*Unified Soil Classification System*
Upslope	70	16	32.5	10	SC
Downslope	44	24	34.3	12	CL-ML

Herron Hill

The Herron Hill landslide is in Lewis

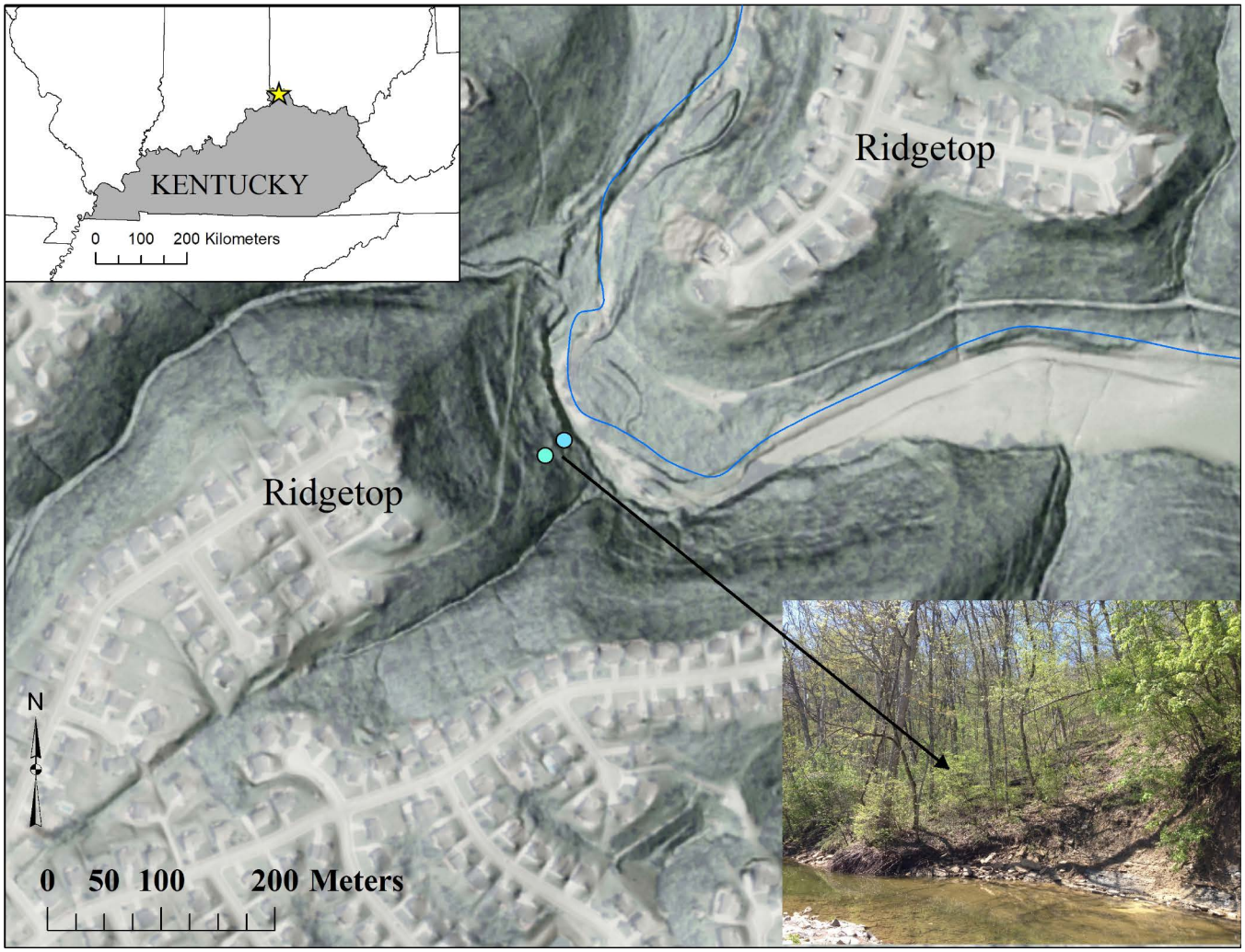

Figure 2. Combined hillshade and aerial photograph of the Doe Run landslide complex. The blue dots indicate the soil-monitoring locations along the slope. The yellow star on the index map indicates the general location of the site. The inset photo is of the toe of the landslide entering the creek below.

County, northeastern Kentucky. The slide area is characterized by steep ridges and conical knobs that are erosional remnants of steep slopes of the Appalachian Basin to the east. This landslide occurs in the Estill Shale Member of the Crab Orchard Formation (Silurian), which consists of greenish gray clay-shale and interbedded limestone. Above the Estill Shale, in ascending order, are the Bisher Limestone (Silurian) and the Ohio Shale (Devonian). The Bisher is a thin-bedded limestone that ranges in texture from finely crystalline to coarse and sandy (Morris, 1965). The Ohio Shale is a fissile carbonaceous shale that weathers easily, which commonly forms vertical fractures. Translational slides and slumps cause repeated road failures in the area where the slope has been overly steepened during construction (Morris, 1965). An old road that cuts across the landslide was abandoned in the mid-1990s because of repeated landslide damage. Seepage is persistent from the slope above the old road. The slope ranges from approximately 16° upslope to approximately 6° at the toe, and several recent small slumps are visible along the slope (Fig. 3). The colluvium that develops on the Estill Shale is primarily a weak and poorly drained silty clay loam. The transition from a thin colluvial cover to weathered clay-shale occurs just a few centimeters below the surface, which makes distinguishing a colluvium-bedrock contact difficult and interpreting the landslide failure zone challenging. Electrical-resistivity measurements indicate a failure zone approximately 2 m below the surface,

Table 3. Field descriptions of colluvial soil at the Doe Run landslide

Upper Pit (Depth, cm)	*Soil Description*
0–10	Dark brown, silty topsoil, organic-rich.
10–20	Light brown, silty clay, soft.
20–50	Light brown to greenish gray, clayey silt; few loose, flaggy rocks.
50–75	Light brown to greenish gray, clayey silt; few loose, flaggy rocks.
Lower Pit (Depth, cm)	*Soil Description*
0–40	Dark brown, loose, silty, organic-rich.
40–70	Light brown, silty clay, soft, wet.
70–100	Light brown to gray, clayey silt; few loose, weathered limestone slabs.
100–130	Light brown to grayish blue, clayey shale, mottled with light gray clay; several loose, weathered limestone slabs; small sticks surrounded by light gray clay.

Table 4. Soil properties at selected soil pits in the Doe Run landslide.

Location	*Depth (cm)*	*Natural Gravimetric Water Content (%)*	*Liquid Limit (%)*	*Plasticity Index (%)*	*Unified Soil Classification System*
Upslope	70	41.2	45.2	27	CH
Downslope	120	43.8	43.9	27	CH

coinciding with a greenish gray to red clay-shale lithology (Crawford and Bryson, 2018).

To describe and classify the soil, two pits (indicated by the blue dots on Figure 3) were dug by a backhoe: one upslope, above the old road, and one downslope, near the toe. Field soil descriptions and index properties are listed in Tables 5 and 6, respectively. Natural gravimetric water contents and Atterberg limits were determined according to ASTM standards D2216 and D4318, respectively. The Unified Soil Classification System designations were determined according to the Natural Resources Conservation Service soils data for Kentucky.

Methodology

Soil-Moisture Sensors

Two types of sensors were used to capture the subsurface hydrologic conditions within the landslides. The first was a water-content reflectometer, which is a multiparameter sensor that monitors the soil's volumetric water content, bulk electrical conductivity, bulk dielectric permittivity, and temperature (Table 7). The sensor has two parallel stainless-steel rods (120 mm long) that were inserted into the upslope exposed soil mass. The water-content data are derived from the rod's sensitivity to the dielectric permittivity of the surrounding soil and the velocity of electromagnetic-wave propagation along the rods (Campbell Scientific Inc., 2014). Water has a significant effect on electromagnetic wave propagation and, in general, greater water content will increase dielectric permittivity. A calibration equation is used to convert period and electrical conductivity to bulk permittivity. In general, volumetric water content can be calculated using several parameters (Eq. 1):

$$\Theta = \frac{V_w}{V} nS = \omega \frac{\gamma_d}{\gamma_w} \quad \text{Eq. 1}$$

where Θ = volumetric moisture content (percent), V_w = volume of water (ft^3 or m^3), V = total volume (ft^3 or m^3), ω = gravimetric moisture content (percent), S = saturation (percent), n = porosity, γ_d = dry unit weight (lb/ft^3 or kN/m^3), and γ_w = unit weight of water (lb/ft^3 or kN/m^3). The water-content reflectometer uses the Topp equation (Eq. 2), which quantifies the relationship between dielectric permittivity and volumetric water content in soils (Topp and others, 1980):

$$\Theta = -5.3 \times 10^{-2} + 2.92 \times 10^{-2} K_a - 5.5 \times 10^{-4} K_a^2 + 4.3 \times 10^{-6} K_a^3 \quad \text{Eq. 2}$$

where Θ = volumetric water content (percent) and K_a = bulk dielectric permittivity. The bulk electrical conductivity measured by the water-content reflectometer is determined by exciting the rods with a known nonpolarizing waveform and measuring the signal attenuation (Campbell Scientific Inc., 2014). Free ions in the soil provide the electrical

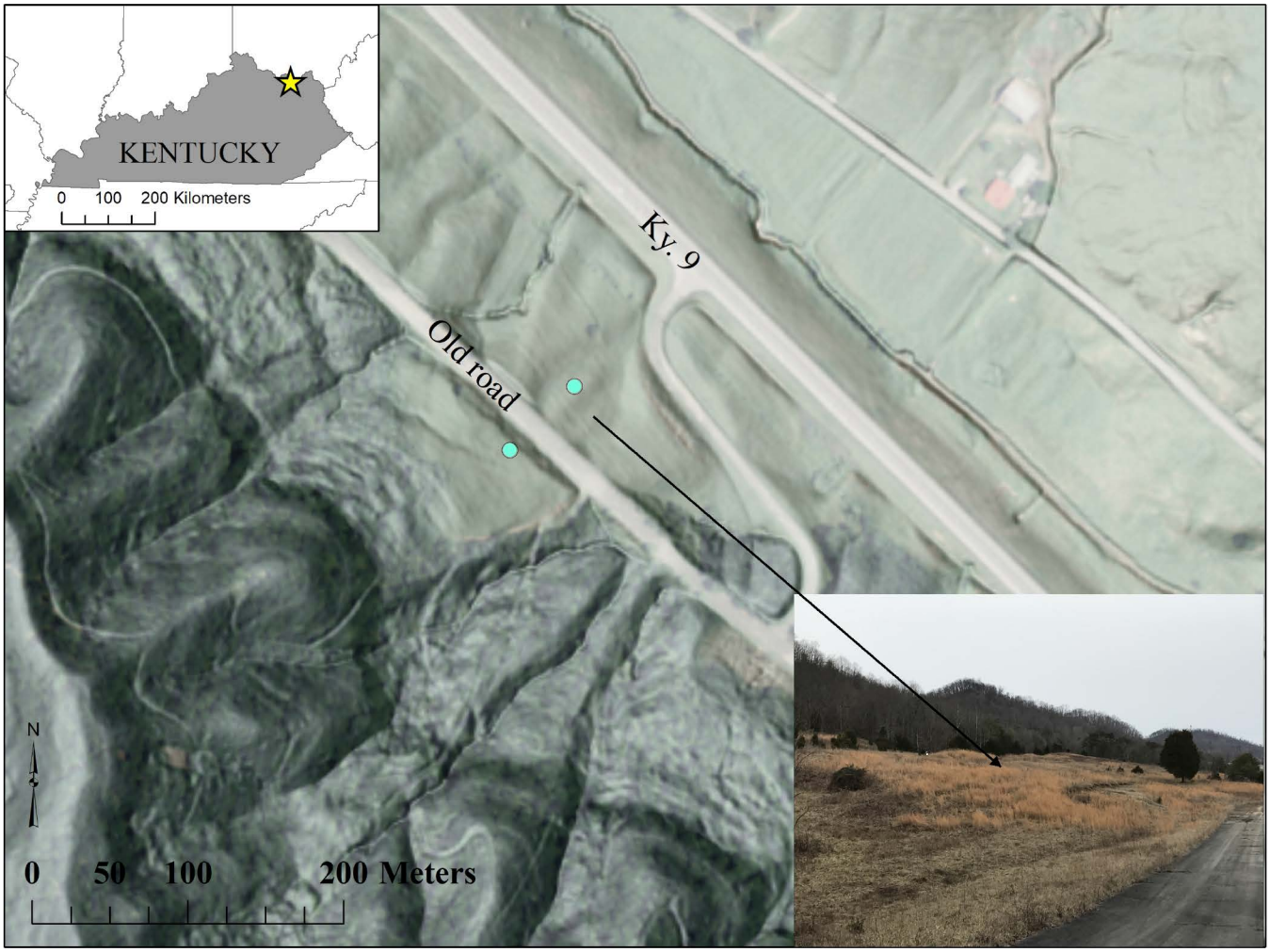

Figure 3. Combined hillshade and aerial photograph of the Herron Hill landslide complex. The blue dots indicate the soil-monitoring locations along the slope. The yellow star on the index map indicates the general location of the site. The inset photo was taken approximately midslope and shows a secondary scarp just above the lower part of the old road.

path, which results in the signal attenuation. Temperature is measured with a thermistor in contact with one of the rods. The rods were inserted horizontally into the undisturbed, upslope face to capture the transient wetting fronts in the soil. The rod probes were easy to insert into the soil by hand at all locations. The relationship between bulk electrical conductivity and its components was described by Rhoades and others (1976) (Eq. 3):

$$\sigma_{bulk} = \sigma_{solution} \Theta_v T + \sigma_{solid} \quad \text{Eq. 3}$$

where Θ_v = volumetric water content (percent), σ_{bulk} = electrical conductivity of the bulk soil, $\sigma_{solution}$ = electrical conductivity of the soil solution, σ_{solid} = electrical conductivity of the solid constituents, and T = soil-specific transmission coefficient.

The other sensor used was a dielectric water-potential sensor for measuring soil-water potential (Table 8). Water potential is the energy state of water in the soil, a determination of stress in the soil based on how water moves—i.e., the negative pore pressures exerted by the soil matrix cause water flow in unsaturated soil (Abramson and others, 2002). Water content and water potential (also called matric suction) are related by a relationship unique to a given soil type, which is expressed by a soil-water characteristic curve (SWCC). The magnitude of the water potential is controlled by surface tension within the pores and grain size (Abramson and others, 2002). The dielectric water-potential sensor uses a known material (ceramic disc) with a static matrix of pores that is buried in the soil, which allows the soil to come into hydrau-

Table 5. Field descriptions of colluvium and weathered bedrock at the Herron Hill landslide	
Upslope Pit (Depth, cm)	*Soil Description*
0–0.3	Dark brown topsoil, blocky, organic-rich.
0.3–0.6	Brown, silty clay loam.
0.6–1.2	Brownish green clay-shale, soft, mottled with reddish brown clay-shale; streaks of sand; few rock fragments.
1.2–2.1	Light blue to greenish gray clay-shale.
2.1–2.7	Reddish brown clay-shale; soft, no structure.
Downslope Pit (Depth, cm)	*Soil Description*
0.0–0.07	Dark brown topsoil, blocky, organic-rich.
0.07–0.15	Brown, silty clay loam, soft, few organics.
0.15–1.2	Brown to gray, silty clay-shale, soft, weathered fissile; few rock fragments, sand stringers.
1.2–1.8	Greenish gray to brown, silty clay-shale, soft to fissile.
1.8–2.1	Light blue to greenish gray clay-shale, hard, moderate structure; thin, sandy stringers.
2.1–2.7	Reddish brown clay-shale, hard, blocky texture.
2.7–3.5	Gray to brown, weathered shale, fissile, soft, crumbly.

Table 6. Soil properties at selected pits in the Herron Hill landslide.

Location	*Depth (cm)*	*Natural Gravimetric Water Content (%)*	*Liquid Limit (%)*	*Plasticity Index (%)*	*Unified Soil Classification System*
Upslope	120	26	44	18	ML
Downslope	120	31	43	14	ML

lic equilibrium (Decagon Devices Inc., 2017). Because the two mediums (disc and soil) are moving toward equilibrium, measuring the water potential of the disc gives the water potential of the soil. This method allows for a wide range of water-potential measurements. Equation 4 determines total soil-water potential (Decagon Devices Inc., 2017) and Equation 5 describes the attraction of water to soil particles, which is similar to matric potential:

$$\Psi_t = \Psi_p + \Psi_g + \Psi_o + \Psi_m \quad \text{Eq. 4}$$

$$\Psi_p = u_a - u_w \quad \text{Eq. 5}$$

where Ψ_t = total soil-water potential and the subscripts t, p, g, o, and m are total, pressure, gravitational, osmotic, and matric, respectively; u_a = pore-air pressure (kPa) and u_w = pore-water pressure (kPa).

The hydrologic sensors were installed in soil pits dug into each landslide, upslope and near each toe (Fig. 4). Three pits were at the Roberts Bend landslide, two pits at Doe Run, and two pits at Herron Hill. The sensors were placed in the undisturbed, upslope face of the exposed soil. As much as possible, the sensors were nested vertically in pairs. A few of the pairs could not be placed at the same depth because of soil stiffness or large rocks. The depths at which the sensors were placed were based on soil-type boundaries (textural or grain-size differences) and ease of installation (Table 9). For the upslope pits at the Doe Run and Roberts Bend landslides, the deeper sensors were placed at the colluvium–weathered bedrock contact.

After the sensors were placed in the ground, the trenches were backfilled. Because of the low power draw and because no calibration was required, both types of sensors were designed to function permanently in the soil.

Rain Gage

Rainfall was measured at each landslide with a tipping-bucket gage and a data logger. The self-

Table 7. Volumetric water-content specifications.		
Parameter	*Range*	*Accuracy*
Volumetric water content (using Topp's equation)	5–50%	±3% volumetric water content typical in mineral soils where solution electrical conductivity ≤ 10 dS/m
Electrical conductivity (bulk)	0–8 dS/m	± (5% of reading + 0.05 dS/m)
Temperature	–10 to +70°C	±0.5°C for sensor buried in soil
Relative dielectric permittivity	1–81	For 1 to 40: ±(3% of measurement + 0.8) for solution electrical conductivity ≤ 8 dS/m 40–80 ± for solution electrical conductivity ≤ 2.8 dS/m

Table 8. Water-potential sensor specifications.	
Range	–9 to –100,000 kPa
Accuracy	±(10% of measurement + 2 kPa) from –9 to –100 kPa

emptying bucket has a diameter of 20.3 cm, which meets National Weather Service specifications. The battery-operated logger has a 1-min resolution, and rainfall was logged at 0.25 mm/tip. Rainfall collection was standalone, and not connected to the system collecting the soil-moisture data. Sensor performance and response to movement of water in the soil are shown in Figure 5, which is a plot of volumetric water content (the last value recorded in each 15-min period) versus rainfall (total for each 15-min period) at the Doe Run landslide. On June 18, 2015, approximately 35.5 mm of rain fell between 7 and 11 p.m. At the time of rainfall, the water-potential sensor in the upslope pit at 70 cm recorded –14 kPa, and all other sensors were recording near the sensor limit of approximately –9 kPa, suggesting the soil was near saturation. For the upslope pit at 30 cm depth, the increase in volumetric water content after approximately 9 mm of rain took just a few minutes. At 70 cm depth, the increase in volumetric water content took about 45 min. For the downslope pit, at the deepest location, there was no response.

Data Collection and Power Supply

To connect the sensors to a data logger, the sensor cables were threaded from each pit together through ¾-in. flexible PVC conduit. The conduit was liquid tight and resistant. The conduit and cables inside it were placed along the surface of the landslide toward an enclosure that housed the

Figure 4. Soil pits, sensor locations, and soil interpretation at the Doe Run landslide upslope (left), the Roberts Bend landslide downslope (middle), and the Herron Hill landslide upslope (right).

Table 9. Slope locations, sensor types, and depth at all landslides. Θ is volumetric water content and Ψ is water potential.

Landslide	*Pit Location and Sensor Type*	*Sensor Depths (cm)*
Doe Run	Upslope Θ	30, 70
	Upslope Ψ	30, 65
	Downslope Θ	75, 130
	Downslope Ψ	55, 130
Herron Hill	Upslope Θ	90, 240
	Upslope Ψ	100, 240
	Downslope Θ	100, 240
	Downslope Ψ	80, 180
Roberts Bend	Above road, upslope Θ	45, 70
	Above road, upslope Ψ	45, 70
	Above road, midslope Θ	30, 65
	Above road, midslope Ψ	30, 65
	Below road, Θ	25, 44
	Below road, Ψ	25, 44

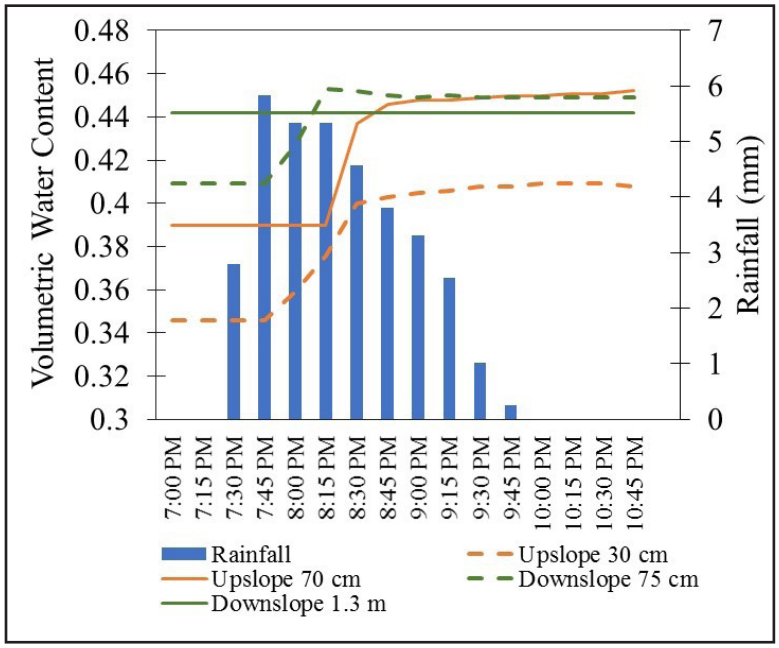

Figure 5. Volumetric water response to rainfall on June 18, 2015, from 7 to 11 p.m. at the Doe Run landslide.

data logger and power source. The enclosures are weather resistant and provided enough space for the data logger, battery or charging regulator, and any excess cable. The enclosures were attached to a hollow steel pole and secured with concrete into the ground at approximately 0.6 m depth (Fig. 6).

Data from the hydrologic sensors were acquired at all sites with data loggers that used an SDI-12 communication protocol. The SDI-12 data-logger acquisition system is characterized by low power requirements, flexible wiring codes and connections, and easy programming. The data logger measures electrical signals and converts the measurements to engineering units. Data were retrieved in the field using a serial cable, and the data were then copied from the data logger to a laptop computer. The program used to acquire data from the sensors did not store every measurement, but rather a combination of measurements in calculated timeframes. The wiring panel contains the voltage terminals, C terminals, and grounding terminals in order to control the actions of the data logger. The program used in the data loggers was written to excite the sensors and take a reading every 15 s, so those data could be retrieved in 15-min, hourly, and daily intervals in downloadable tables. The hourly and daily tables use an average value, maximum, and minimum for those intervals. The last value for an interval is used to represent each 15-min interval. Table 10 lists selected data collected at the sites. The data-logger starter software we used (campbellsci.com/pc200w) for data collection and compilation is downloadable, free, compatible with the sensors used in this project, and designed for relatively simple data-monitoring and collection programs.

The hydrologic sensors and data-acquisition system are powered by a 12-volt charging regulator. It includes a 7-amp-hour lead-acid battery and charging regulator. The exception was the system at the Roberts Bend landslide, which instead used a sealed, rechargeable, 12-volt, 7.2-amp-hour battery. Charging power was supplied by a 10-watt solar panel. The whole power-supply system balances the charging source (solar panel) and the load as the battery nears a

Figure 6. Example of a field station at the Roberts Bend landslide. The enclosure contains a data logger and battery, which is charged by a 10-watt solar panel.

Table 10. Data tables and parameters collected at each landslide.

Data Tables	*Parameters*	*Units*
15-min Hourly (average) Daily (average)	Volumetric water content	%
	Electrical conductivity	dS/m
	Temperature	°C
	Water potential	kPa

full charge, and the regulator reduces the current drawn from the source. This is important considering the wooded environment and seasonal fluctuation in sunlight. The solar panel was mounted on the pole above the enclosure and oriented south to face the equator at a tilt angle of approximately 48°, based on the latitude of the landslides.

Observations

Rainfall and Landslide Activity

Average annual statewide cumulative rainfall from 2014 to 2018 was 53.1 in., recorded by the Kentucky Mesonet (www.kymesonet.org/summaries.html) (Table 11). Cumulative rainfall for 2016 and 2017 was slightly above the 5-yr average, but 2018 was significantly greater. This may explain the overall higher volumetric water contents, short-lived drying periods (particularly in the sensors buried at deeper locations), and the increase in landslide occurrence in 2018 compared to previous years. A plot of statewide average rainfall and documented landslides from the KGS Landslide Inventory shows the unsurprising trend that years with more rainfall correlate with years of increased landslide occurrences (Fig. 7). The largest one-day rainfall during the monitoring period was 63.5 mm at Roberts Bend, 88.9 mm at Doe Run, and 78.7 mm at Herron Hill. The rainfall measured at each landslide for a year is generally close to the statewide average.

To illustrate the relationship between rainfall, soil moisture, and landslide movement, we installed a cable extension transducer at the Roberts Bend landslide. Also referred to as a wire extensometer (Coe and others, 2003), the CET is a stainless-steel cable that measures absolute linear positions. It was attached to a potentiometer enclosed in a protective case. The CET output signal was voltage, which was then converted to linear displacement. One end of the CET was on what was assumed to be a stable part of the slope, stretched from there across the landslide's toe bulge, where the other end was anchored to a pole in the ground. The CET thus recorded extension and retraction movements.

Table 11. Statewide average cumulative rainfall across Kentucky. From the Kentucky Mesonet (www.kymesonet.org).

Year	*Cumulative Rainfall (mm)*
2018	1,570
2017	1,272
2016	1,286
2015	1,452
2014	1,165

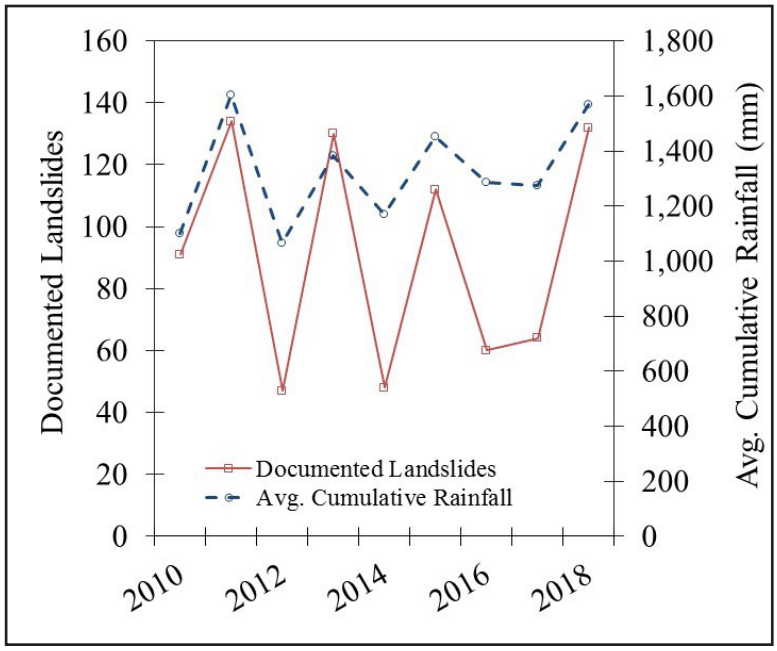

Figure 7. Average cumulative rainfall and documented landslides in Kentucky.

The total movement of the landslide over the monitored period (late October 2015–late April 2019) was approximately 4.5 cm. An analysis of the cumulative horizontal displacement of the toe of the landslide showed seasonal periods of movement with varying average velocity (Fig. 8) separated by a period with little movement. The CET is limited to a linear position along a horizontal line, so the deviations (positive movements and peaks shown in Figure 8) from shortening may result from various causes: ground rotation causing the anchor pole on the bulge to rotate backward, ground rotation that causes the CET pole to rotate forward, ice on the cable, soils expanding because of moisture changes, or thermal changes in the CET cable.

A plot of CET movement and volumetric water from Nov. 24–Dec. 29, 2016, a period spanning the drying period to a wetting phase (Fig. 9), shows the CET recorded a minor amount of movement at the end of the dry period, followed by a sharp increase (approximately 0.4 cm) in cumulative displacement, and then a leveling out that coincided with several rainfalls. The sharp decrease in cumulative displacement (i.e., when the slide advanced less) occurred as the soils

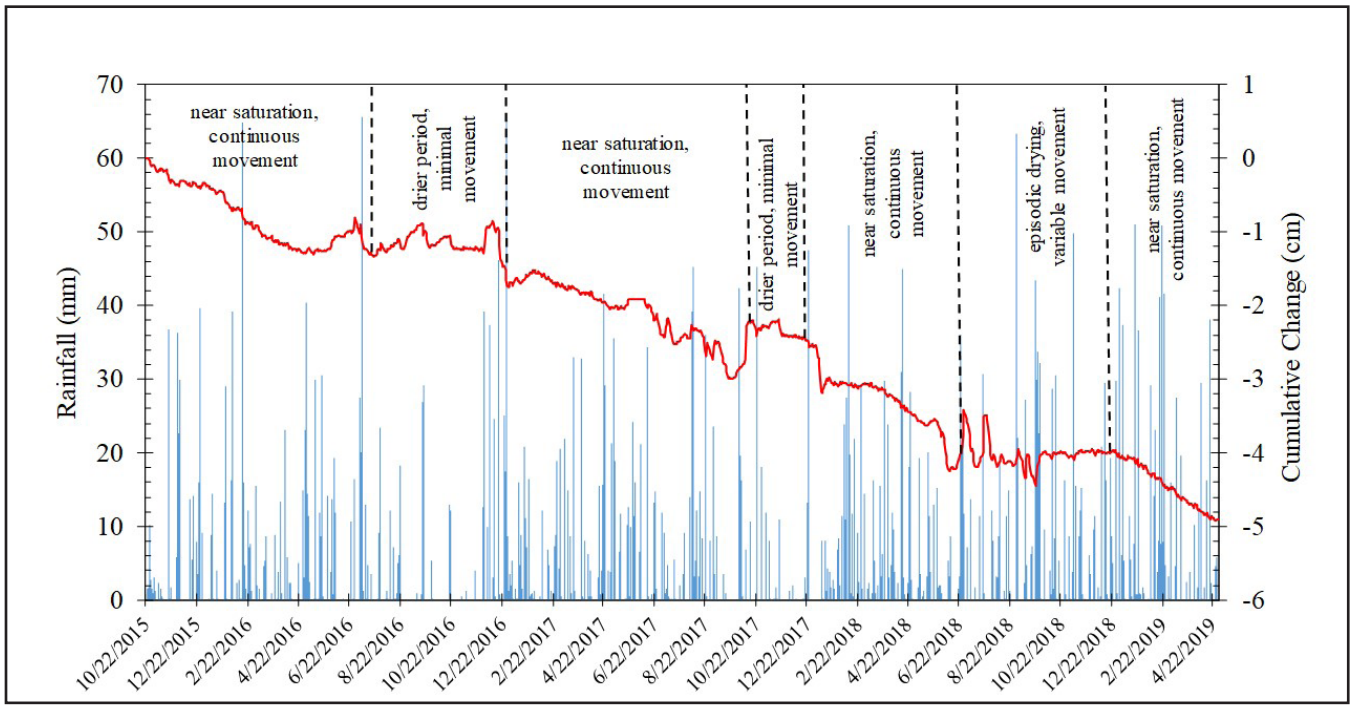

Figure 8. Cumulative horizontal displacement measured by CET (red line) and rainfall at the Roberts Bend landslide. Periods of increased velocity (sharp decreases in cumulative change) mostly correspond with the wettest multiday storms. Modified from Crawford (2018).

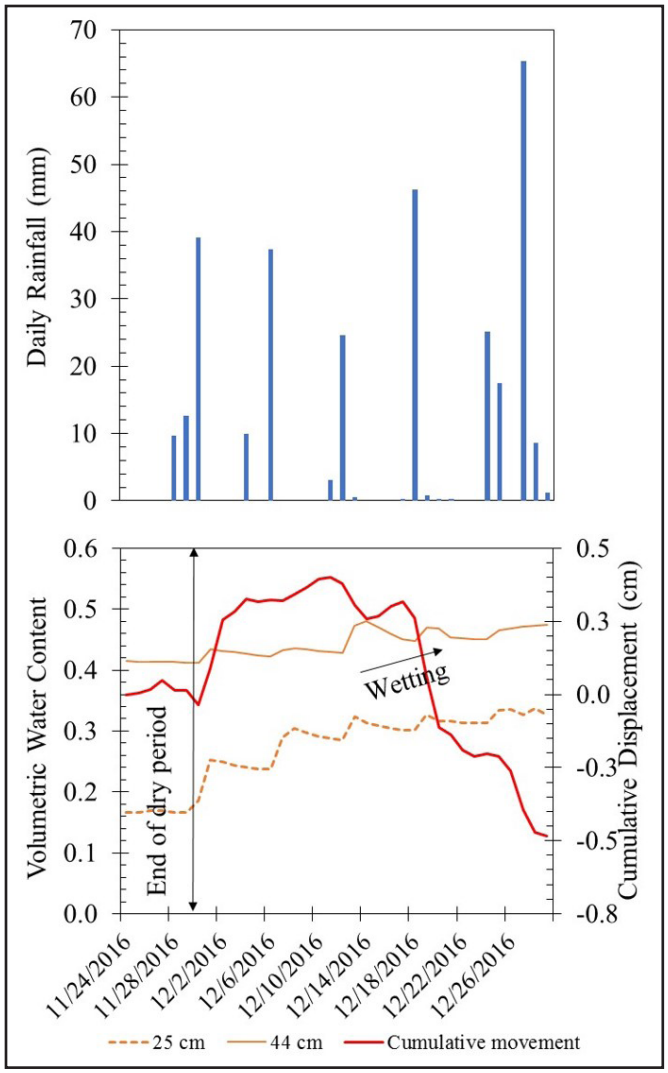

Figure 9. Volumetric water content (orange lines) and horizontal displacement (red line) during a transition from dry through a wetting phase, toward near-saturated conditions, in late 2016 at the Roberts Bend landslide. Cumulative displacement continued by late December (Crawford, 2018).

became wet and trended toward near-saturated conditions.

Soil Moisture

Volumetric water content and water potential were measured along different parts of the slope and at various depths to account for clear seasonal wetting and drying periods. Seasonal fluctuations in the soils' volumetric water content indicated distinct periods of wetting and drying during the year; drying generally took place during the meteorological summer and fall, because of less rainfall and likely in response to increased evapotranspiration (Czikowsky and Fitzjarrald, 2004). The duration and magnitude of drying and wetting paths in the soil were different for each slope location and soil depth, suggesting that differences in soil texture, porosity, and permeability contributed to the soil-moisture profile. Generally, there was one drying period at each landslide a year. In 2016, the drying period was from approximately mid-August to early December at Herron Hill and Roberts Bend. The drying periods at Doe Run for 2016–2018 were from early June to mid-October. The drying periods for all landslides in 2017 and 2018 were shorter, started earlier, and depending on slope location and sensor depth, did not occur at all (water potential did not deviate from the –8 to –9 kPa sensor limit). In 2018, midslope and downslope water-potential sensors at Roberts Bend never exceeded –25 kPa. Water-potential sensors at Doe Run measured –168 kPa upslope and –146 kPa downslope. At other times of the year (nondrying periods), the volumetric water content fluctuated only slightly with each rainfall, but generally maintained a level of near-saturated or saturated conditions. Figures 10–20 show rainfall, volumetric water content, and water potential at all the landslides at different slope locations and soil depths. The colluvial soils in this study stayed saturated or nearly saturated for much of the year, which demonstrates that antecedent moisture affects the rate and depth of transient infiltration during and after rainfall.

Soil-Water Relationships

Correlation of volumetric water content with water potential is an important soil-water relationship known as a soil-water characteristic curve (Fig. 21). Soil-water characteristic tests are used to estimate various soil parameters and describe the behavior of unsaturated soil (Fredlund and Xing, 1994). This relationship indicates pore-space distribution in the soil (size and interconnectedness), which is critical for understanding landslide dynamics. A nonlinear increase in strength as the soil desaturates (dries) is a result of a decrease in water potential. Thus, shear strength of unsaturated soil should be related to the SWCC.

Field Soil-Water Characteristic Curves

In-situ soil systems are partially saturated and exhibit fluctuations in water potential, which is the difference between the pore-air pressure and the

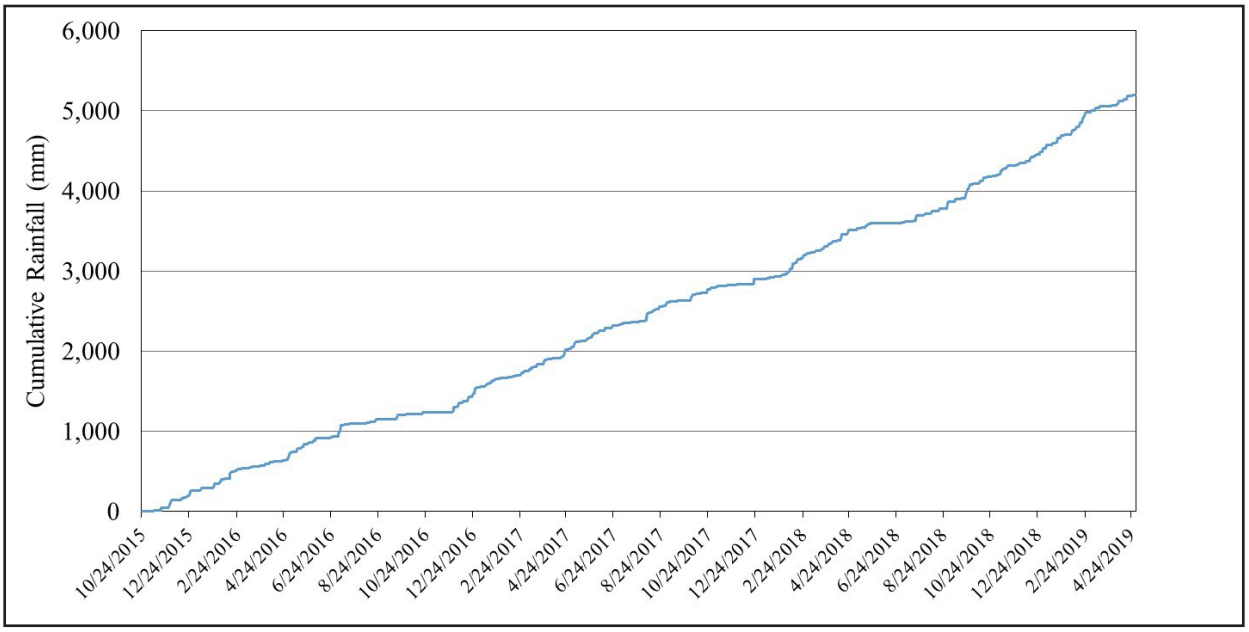

Figure 10. Cumulative rainfall at the Roberts Bend landslide from late October 2015 to late April 2019.

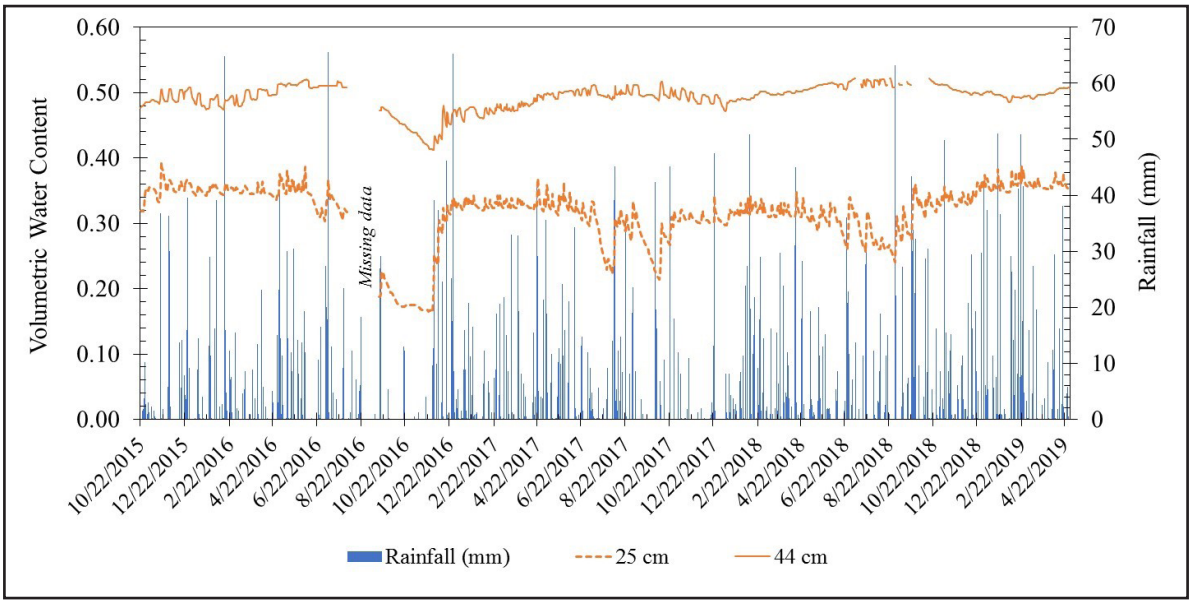

Figure 11. Volumetric water content below the Forest Service road at the Roberts Bend landslide.

pore-water pressure (i.e., $u_a - u_w$). Data from the in-situ soil sensors were used to construct field SWCCs that show wetting and drying paths, also known as the hysteresis effect, in the soil over time (Fig. 22). An absolute value of water potential was used in order to plot on a logarithmic scale in which a higher number indicates drier soil.

Modeled Soil-Water Characteristic Curves

Soil-water data can be fitted to several models (Fredlund and Xing, 1994; Fredlund and others, 2011; Lu and others, 2014; Bordoni and others, 2017; Crawford and Bryson, 2018) that result in curves for conditions from saturated to dry. An analysis of wetting curves for soils may provide insight into slope conditions that trigger landslides (i.e., positive pore pressures that indicate the in-

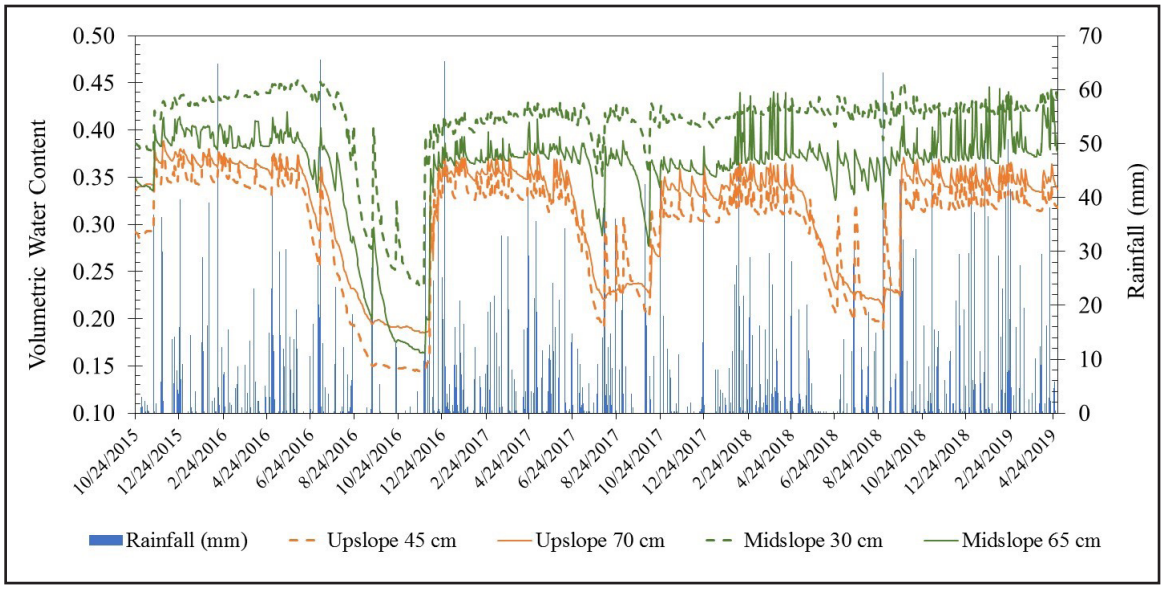

Figure 12. Volumetric water content above the Forest Service road at the Roberts Bend landslide.

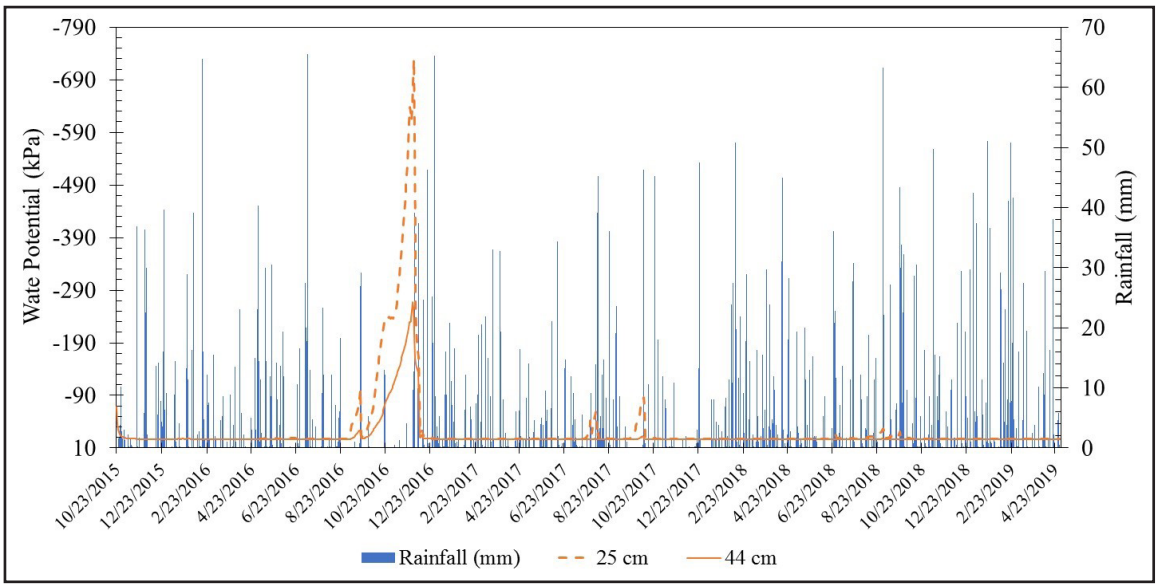

Figure 13. Water potential below the Forest Service road at the Roberts Bend landslide.

creased likelihood of a landslide). For this study, however, we used drying-path data to analyze hydrologic relationships, compare field conditions to empirical relations, and establish new models for assessing stress-state variables. The wetting curves contain sharp fluctuations and represent a short amount of time compared to the drying curves, which have a wide range of values, exhibit a clear indication of saturation stages, and a clear linear correlation between volumetric water content and water potential within the primary transition zone (Fig. 23). The field SWCCs were modeled using the Van Genuchten (1980) equation for volumetric water content as a function of water potential (Eq. 6):

$$\Theta = \Theta_r + \frac{(\Theta_s - \Theta_r)}{\{1 + [\alpha (u_a - u_w)]^n\}} \quad \text{Eq. 6}$$

where Θ = volumetric water content, Θ_s = saturated volumetric water content, Θ_r = residual volumetric water content, n = fitting parameter, m = fitting parameter, and α = fitting parameter.

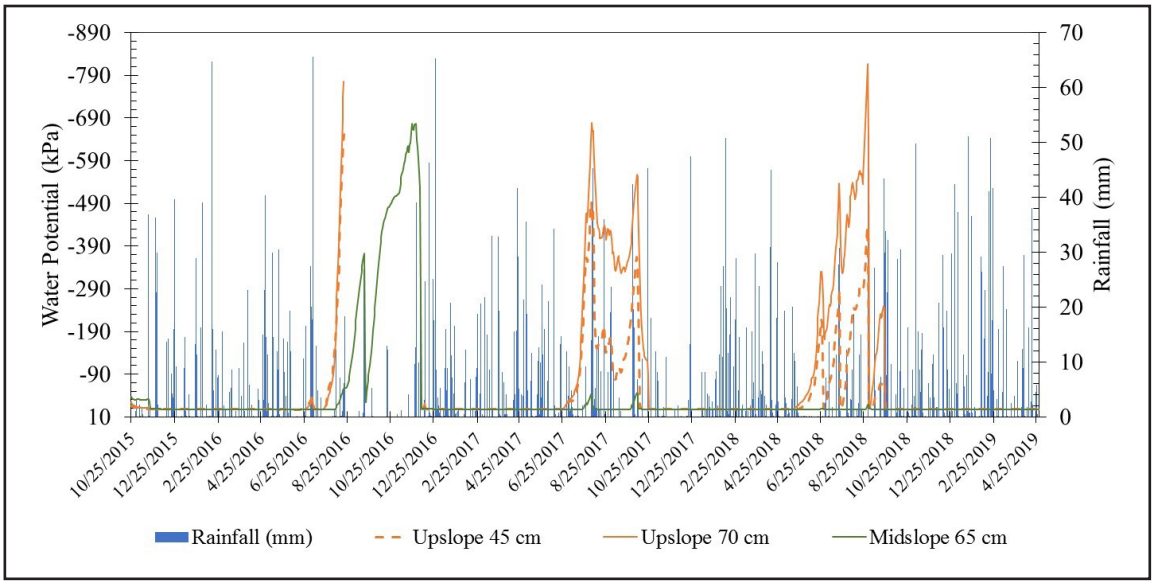

Figure 14. Water potential above the Forest Service road at the Roberts Bend landslide.

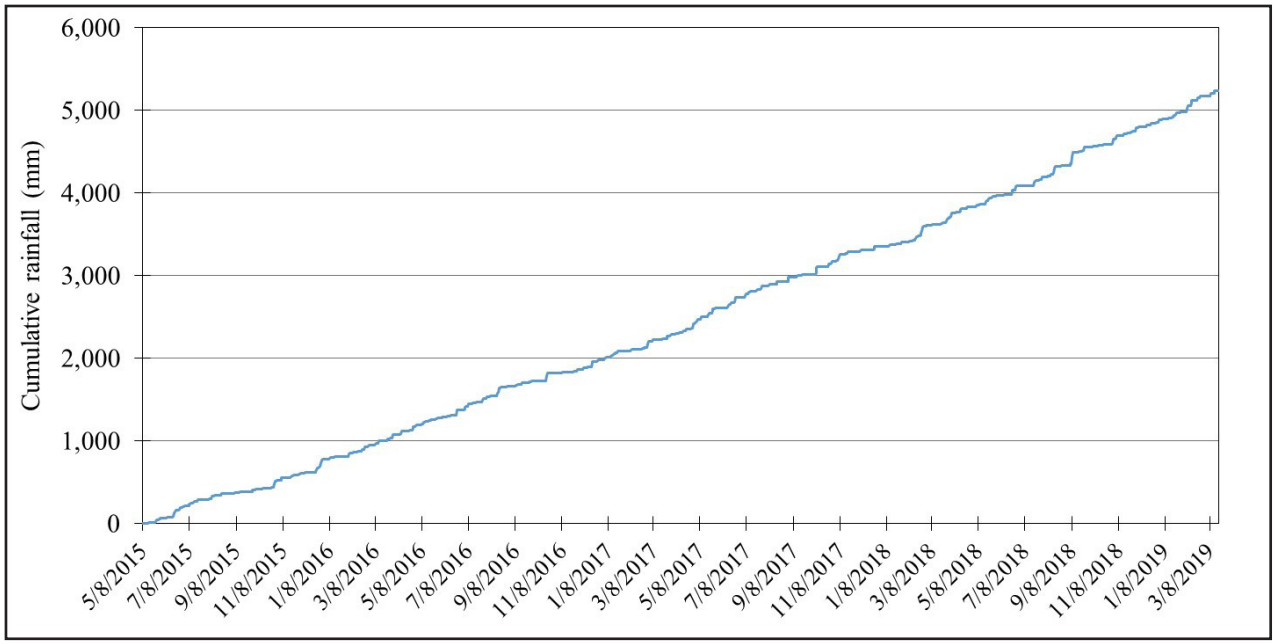

Figure 15. Cumulative rainfall at the Doe Run landslide from early May 2015 to early March 2019.

Relationship With and Implications for Shear Strength

We modeled the influence of pore-air pressure in unsaturated soils using the Mohr-Coulomb shear-strength model. It is based on two independent stress-state variables: net normal stress and water potential (Eq. 7):

$$\tau_{ff} = c' + (\sigma - u_a)\tan\varphi' + \frac{\Theta - \Theta_r}{\Theta_s - \Theta_r}(u_a - u_w)\tan\varphi' \quad \text{Eq. 7}$$

where τ_{ff} = shear strength, c' = cohesion at zero matric suction (water potential) and zero net normal stress (effective cohesion), $(\sigma - u_a)$ = net normal stress, $(u_a - u_w)$ = matric suction (water potential), Θ_s = saturated volumetric water content, Θ_r = residual volumetric water content, u_a = pore-air pres-

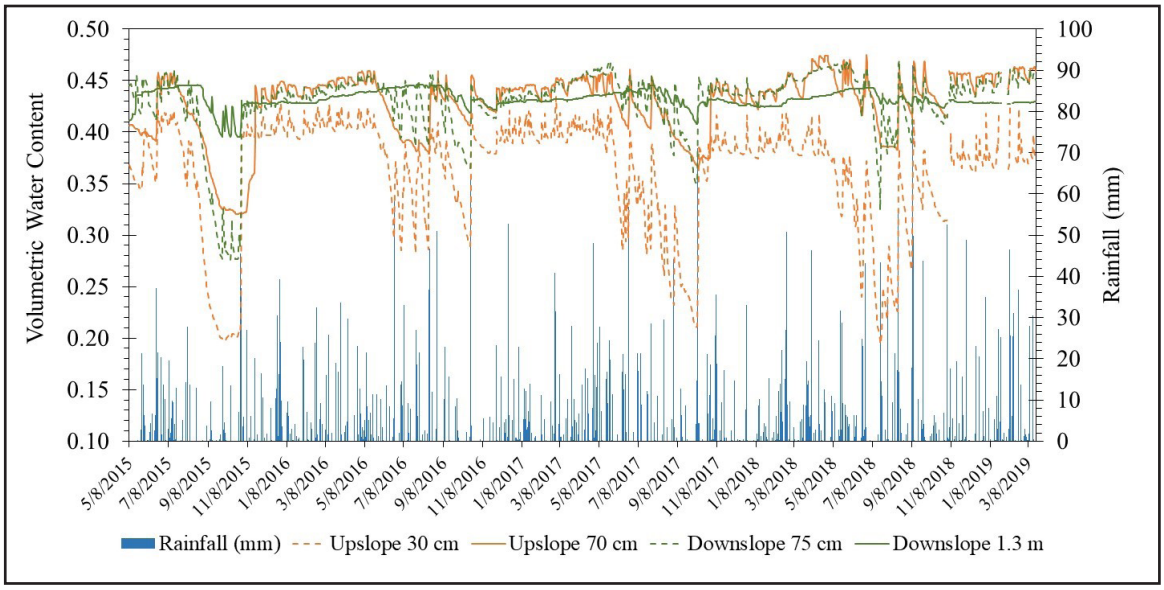

Figure 16. Volumetric water content, upslope and downslope, at the Doe Run landslide.

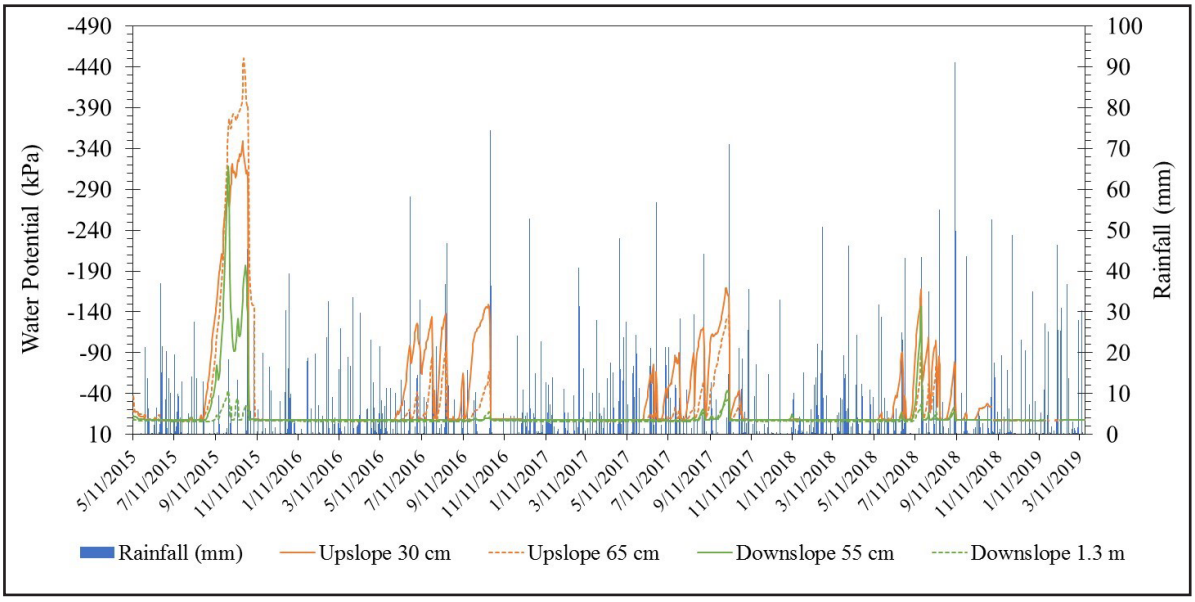

Figure 17. Water potential, upslope and downslope, at the Doe Run landslide.

sure, u_w = pore-water pressure, σ = total stress, and φ' = angle of internal friction associated with net normal stress.

Specifically, the model determines the influence of pore-air pressure within the effective stress component of the more common Mohr-Coulomb saturated shear-strength model (Abramson and others, 2002). For unsaturated soils, volumetric water content and water potential reflect that negative pore pressures (suction) change to positive pore pressures when there is increased rainfall; these parameters are pertinent to investigating the stability of shallow colluvial landslides that are triggered or reactivated by rainfall. Shear-strength parameters were determined from standard CU (consolidated undrained) triaxial tests in accordance with ASTM method D4767 on samples from the Doe Run and Herron Hill landslides. Triaxial tests are reliable and the principal means of obtaining shear-strength data for soils. The CU test is one of the most common types of triaxial tests, and it is used to determine the undrained and drained

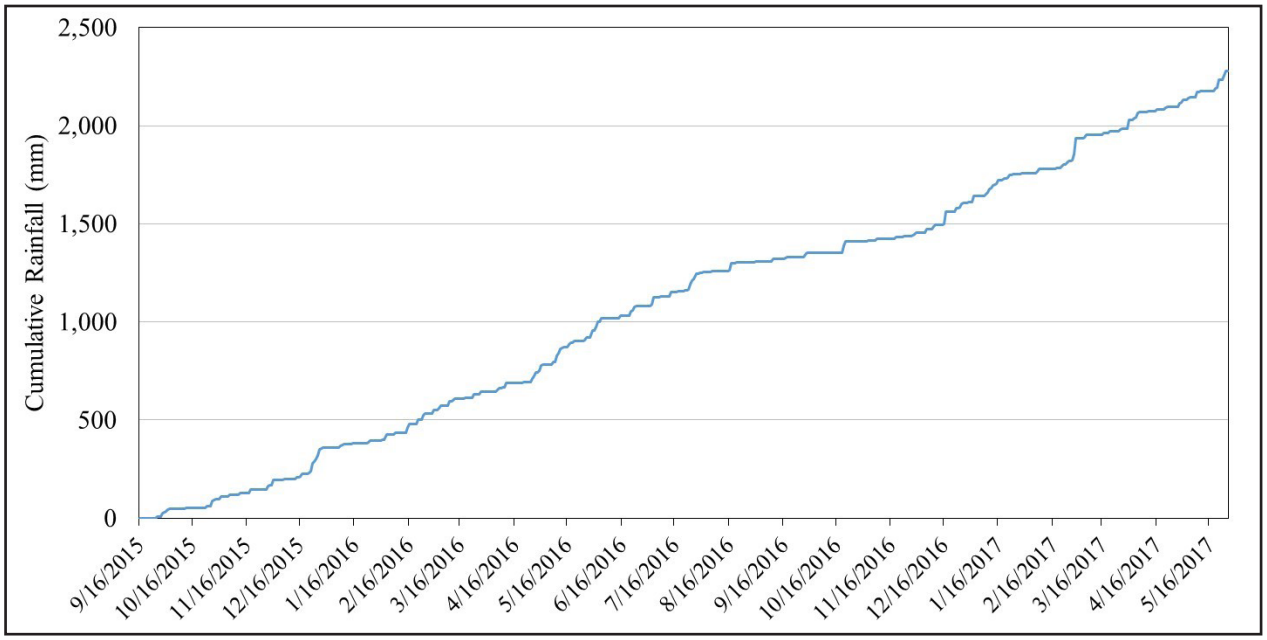

Figure 18. Cumulative rainfall at the Herron Hill landslide from mid-September 2015 to mid-May 2017.

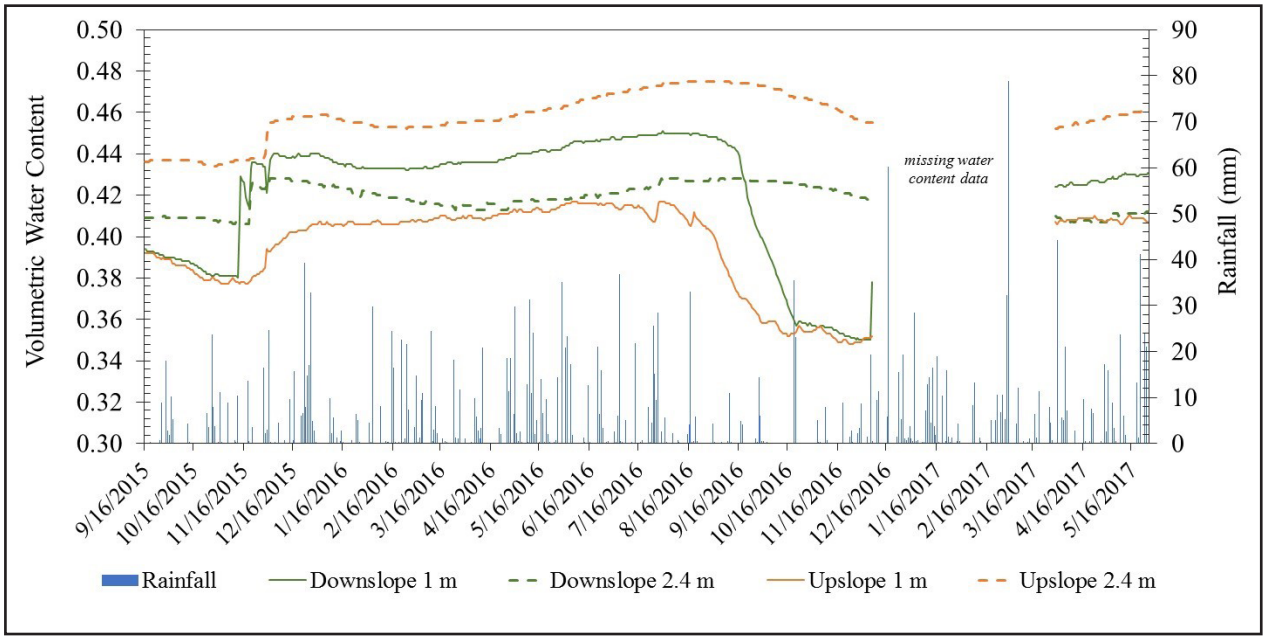

Figure 19. Volumetric water content, upslope and downslope, at the Herron Hill landslide.

shear-strength parameters, including cohesion and internal angle of friction (Budhu, 2007; Das, 2010). We conducted three separate tests of soil samples from each landslide. Each field sample was remolded into a test cylinder in the same way, based on the in-situ dry density and moisture content. Each test is conducted with a different effective consolidation stress, which results in points of maximum shear stress. We used effective stress values of 20, 30, and 40 psi and estimated that these values were greater than what was used to make the test sample. Shear-strength parameters used in this study are listed in Table 12. We used only the peak values of the internal angle of friction and cohesion. Peak values are stress states, as opposed to critical state values, which are a material property needed for

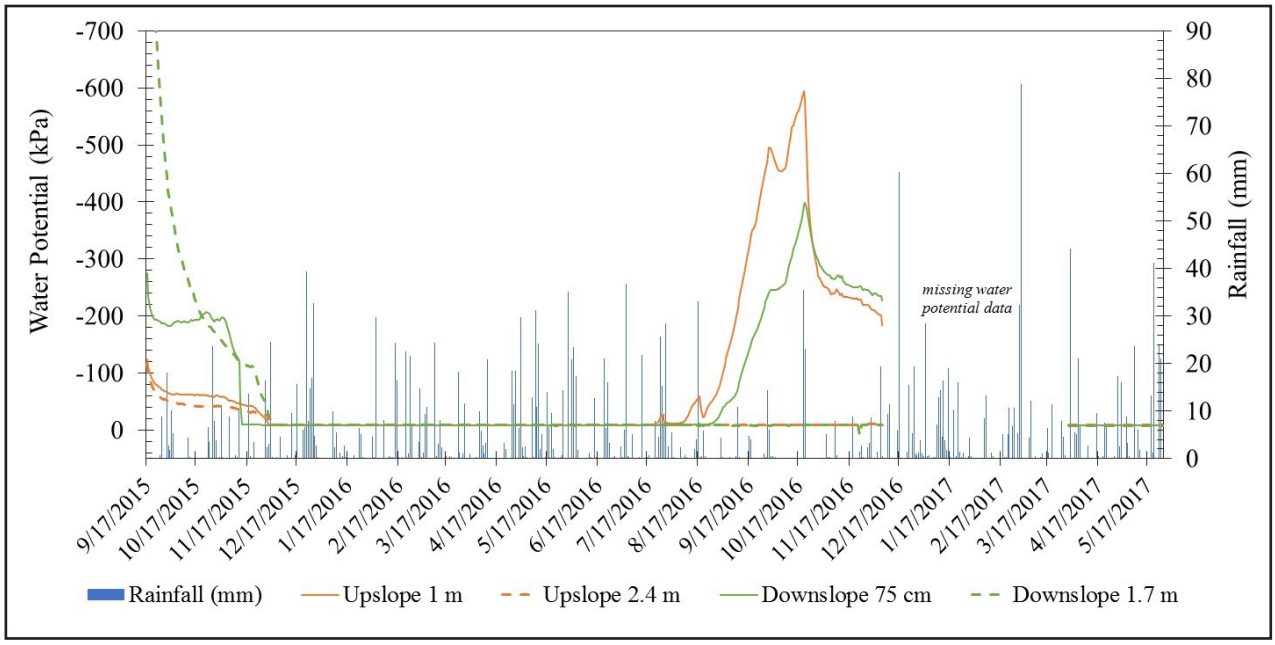

Figure 20. Water potential, upslope and downslope, at the Herron Hill landslide.

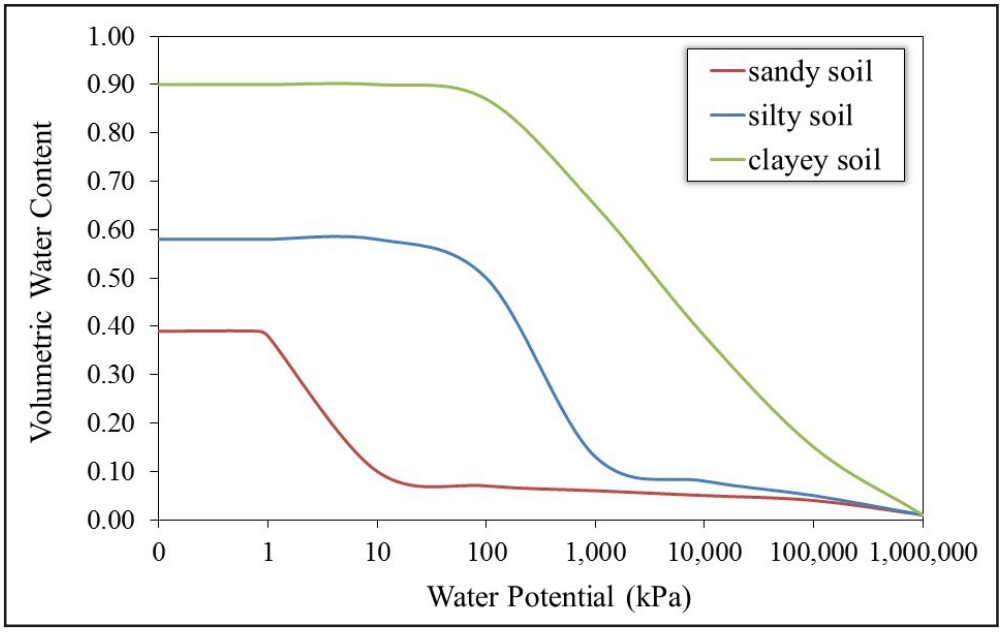

Figure 21. Typical soil-water characteristic curves for sandy, silty, and clayey soils (data from Fredlund and Xing, 1994).

shear-strength models. The colluvial soils tested for in this study are normally consolidated to lightly overconsolidated soils, however, so the peak shear-strength values (φ' and c') are about equal to the critical-state shear-strength values.

Figure 24 shows the in-situ shear-strength data, as interpreted by the Vanapalli and others (1996) shear-strength equation, for all three landslides. These data correlate with the daily average in-situ water-potential values along the drying path. Figure 24 shows that the shear strength increases as water potential increases (soil becomes drier). Shear-strength values range from less than 10 kPa at the Roberts Bend landslide to more than 250 kPa at the Herron Hill landslide.

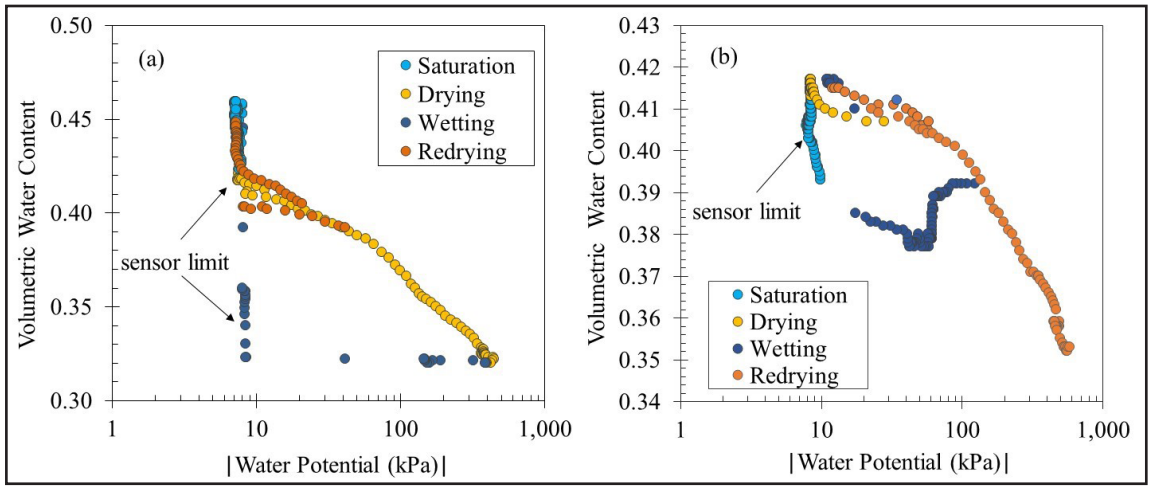

Figure 22. Field soil-water characteristic curves for (a) the Doe Run landslide upslope at a depth of 70 cm and (b) the Herron Hill landslide upslope at a depth of 90 cm. Each dot represents a daily average. The vertical distribution of wetting and saturation points, at approximately 9 kPa, represents the limit of the water-potential sensor (Crawford, 2018).

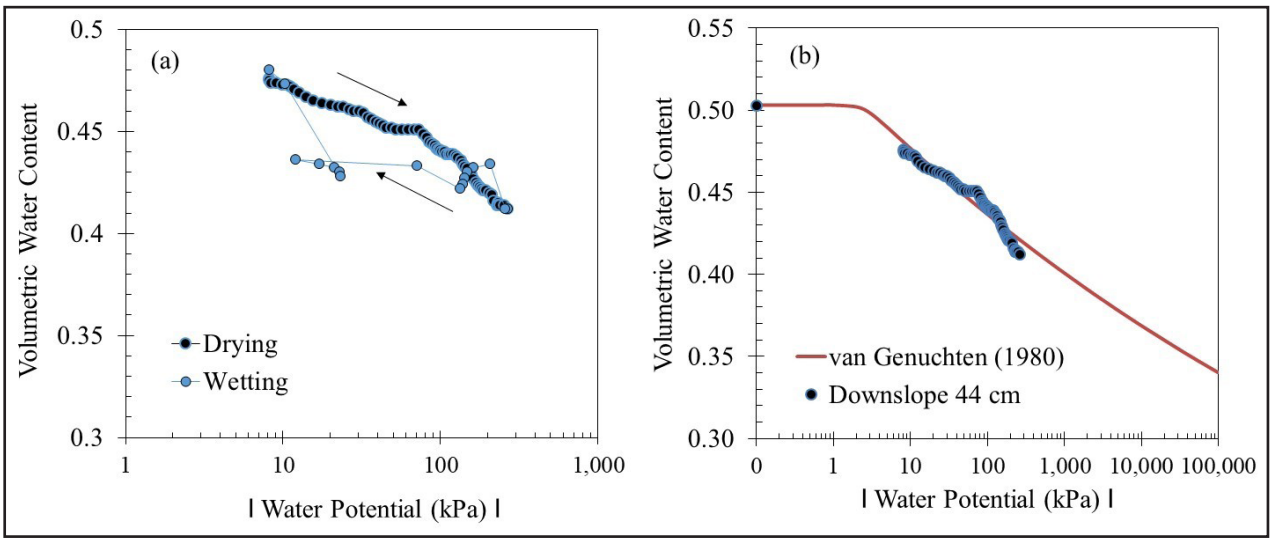

Figure 23. Soil-water characteristic curve for soil downslope at 44 cm depth at the Roberts Bend landslide (a), demonstrating the hysteresis effect of wetting and drying paths, and (b) the modeled curve using the drying path. Each point is a daily average value and represents the transition part of the curve. An absolute value of water potential is used to plot on a logarithmic scale in which a higher number indicates drier conditions. From Crawford (2018).

Table 12. Shear-strength and volumetric-water-content parameters used in equation 7. Shear-strength parameters were determined from standard consolidated undrained tests in accordance with ASTM method D4767. Test samples were remolded soil samples prepared by a static compaction machine.

Landslide	*c′ (kPa)*	*$(\sigma - u_a)$ (kPa)*	*ϕ' (degree)*	*Location*	Θ_s	Θ_r
Doe Run	9.6	13	22	upslope 70 cm	0.44	0.09
				downslope 1.3 m	0.43	0.08
Herron Hill	1.3	29.9	27	upslope 1 m	0.41	0.08
				downslope 1 m	0.44	0.09
Roberts Bend	10.0	8.3	24	downslope 44 cm	0.50	0.10

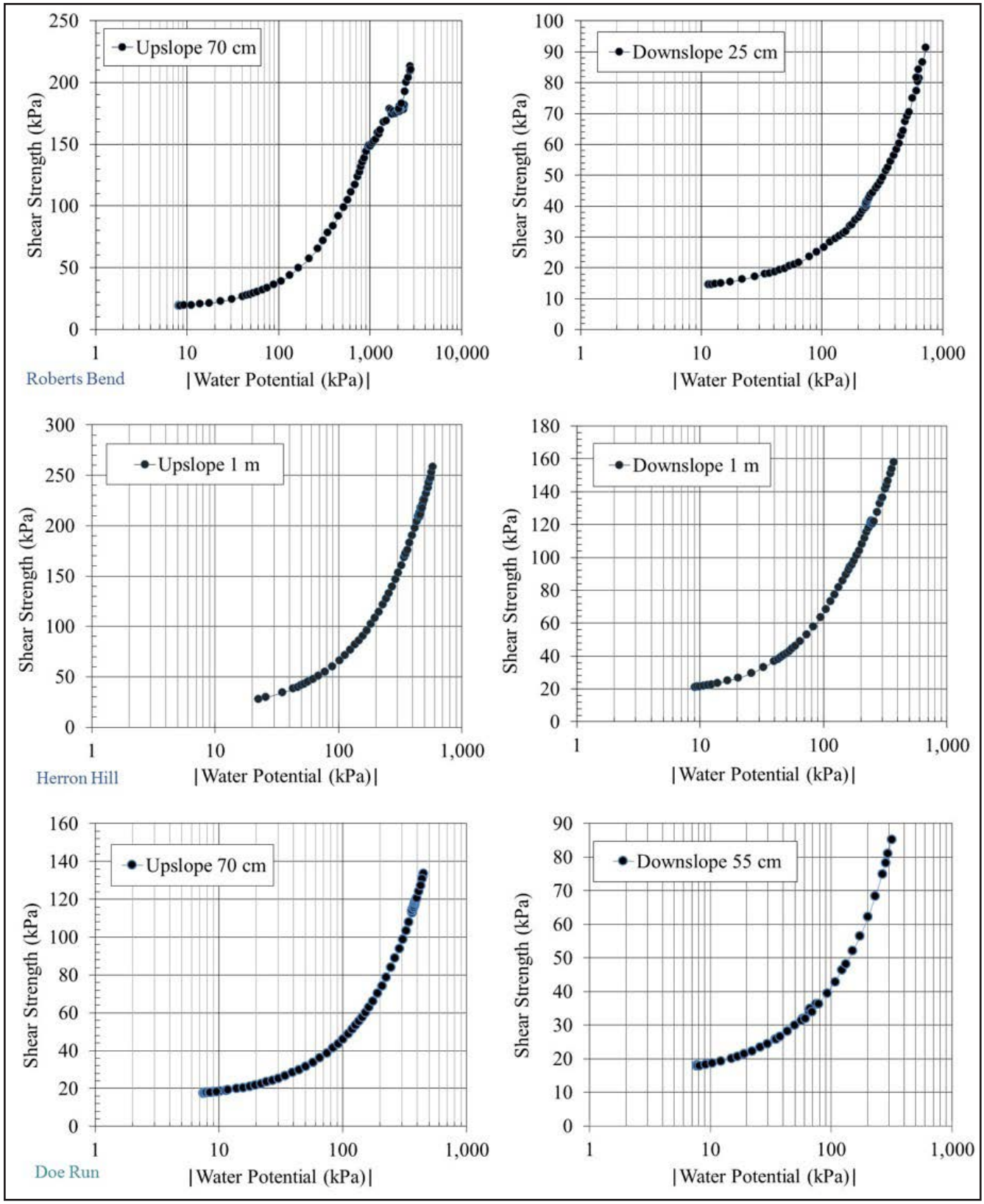

Figure 24. Shear strength and water potential for all three landslides at various locations and depths. Each dot represents a daily average along the drying path. An absolute value of water potential was used in order to plot on a logarithmic scale (higher number is drier).

Suction Stress

The effective degree of saturation and suction stress can be derived from the measurement of volumetric water content and water potential in a landslide. The relationship between effective degree of saturation and suction stress is a form of an SWCC known as a suction stress characteristic curve (SSCC). This relationship indicates differences in soil type and how water moves through the soil, and is often used as a predictor of shear strength (Vanapalli and others, 1996; Guan and others, 2010). The effective degree of saturation (S_e) is a normalized volumetric water content, is unitless, and calculated as shown in equation 8:

$$S_e = \frac{\Theta - \Theta_r}{\Theta_s - \Theta_r} \quad \text{Eq. 8}$$

where S_e = effective degree of saturation, Θ = measured volumetric water content, Θ_s = saturated volumetric water content, and Θ_r = residual volumetric water content.

Suction stress is the product of effective saturation and water potential, and can vary within the unsaturated zone depending on soil type, moisture conditions, and depth below the surface. As in the colluvial soil, in the unsaturated zone the moisture conditions are anisotropic relative to changes in grain fabric and degree of saturation, thus making moisture condition an important factor for slope movement (Lu and Likos, 2006). Suction stress (Lu and Godt, 2013; Chen and others, 2017) can be expressed as:

$$\sigma^s = \frac{\Theta - \Theta_r}{\Theta_s - \Theta_r}(u_a - u_w) \quad \text{Eq. 9}$$

where σ^s = suction stress, $(u_a - u_w)$ = water potential, u_a = pore-air pressure, and u_w = pore-water pressure.

As the soil becomes more saturated, suction stress is reduced and can contribute to triggering landslides (Bittelli and others, 2012). In clayey soils, which have a wide range of water-potential values, suction stress during infiltration could be reduced by as much as 500 kPa because of the low permeability of these soils (Lu and Godt, 2013). Analyzing suction stress over time and correlating it with rainfall can be a proxy for changes in effective stress in a hillslope soil during wetting and drying (Lu and Likos, 2004; Lu, 2008; Lu and others, 2010; Lu and Godt, 2013; Dong and Lu, 2017).

Although the typical relationship represented in an SSCC is between effective degree of saturation (S_e) and suction stress, electrical conductivity can also be used to replace S_e in order to convey information about variable moisture conditions in the soil. Given the linear relation between in-situ volumetric water content and electrical conductivity, electrical conductivity can be assumed to be normalized in a manner similar to that of water contents in soil-water characteristic curves (Crawford and Bryson, 2018; Crawford and others, 2019). Figure 25 is an SSCC constructed from in-situ electrical conductivity from the midslope and downslope locations at the Roberts Bend landslide. For the midslope location at 70 cm deep, the curve can clearly be divided into moisture regimes of transient water behavior, from saturated to dry. The saturated zone exhibits consistent volumetric-water-content and electrical-conductivity values, and as the soil dries, and suction stress and water potential reach the air-entry value, capillary interparticle stresses develop. The transition zone is defined by the range of in-situ measurements, with suction stresses ranging from 200 kPa to approximately 7 kPa. The shape of the curve changes in this zone depending on the soil location and soil type. The residual regime consists of high values of suction stress and water potential and minor changes in volumetric water content and electrical conductivity. The nonlinear curves can be used to estimate permeability, water storage, and shear-strength functions.

Summary

Three landslides in Kentucky were monitored between October 2015 and February 2019. The landslides occur in different physiographic regions, as well as different geologic settings. Each landslide was interpreted to be part of a broad complex exhibiting translational and rotational processes, as well as having nested areas of variable movement. The research focused on landslide characterization, cost-effective field methodologies, and data-collection techniques that can be used to assess hillslope soil-moisture conditions. We measured rainfall, volumetric water content, water potential, and electrical conductivity at various locations

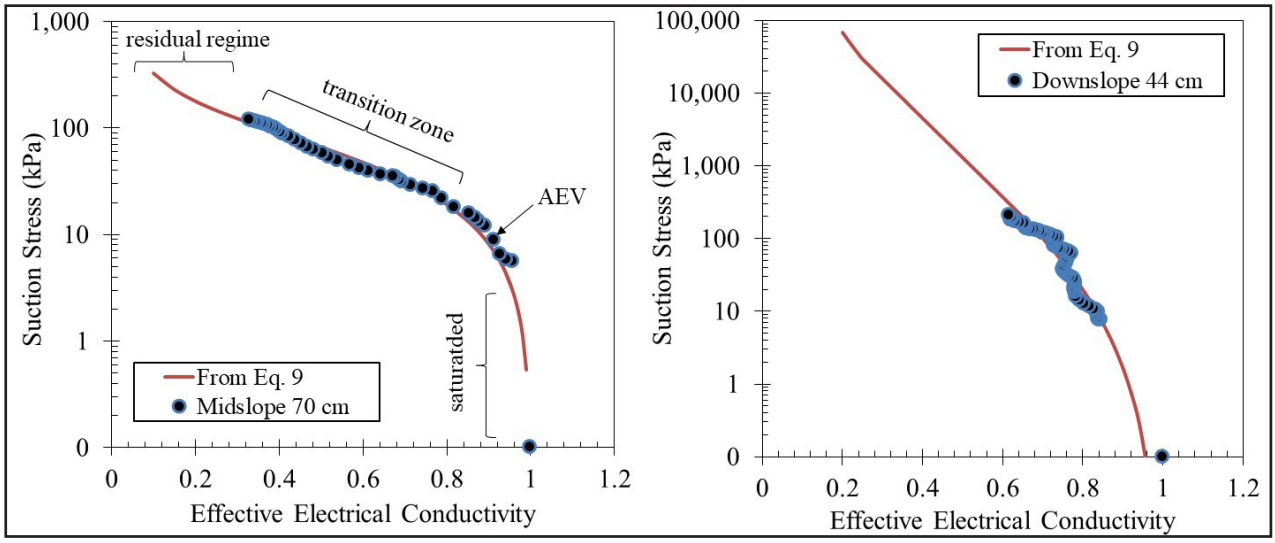

Figure 25. Suction stress as a function of electrical conductivity at two locations at the Roberts Bend landslide. From Crawford (2018).

across the slope, which indicated distinct, seasonal periods of wetting and drying. The duration and magnitude of drying and wetting paths within the soil were different for each slope location and soil depth, suggesting that differences in slope morphology, soil texture, and porosity influence the transient infiltration process. Generally, the shallower the sensor, the quicker the increase in volumetric water content following a rainfall; the deeper the sensor, the less fluctuation in volumetric water content. The downslope locations at Roberts Bend and Doe Run showed very little fluctuation in moisture content and, in 2018 and early 2019, there was no discernible increase in water potential (which indicates no discernable drying). The downslope locations at these landslides are where the most displacement is observed. The monitoring period for Herron Hill was shorter than for the other two landslides, but similar trends in seasonal moisture fluctuation were apparent there as well.

Landslide movement measured at the Roberts Bend landslide was correlated with rainfall and volumetric water content. The total movement (cumulative horizontal displacement at the toe) was approximately 4.5 cm (late October 2015–late February 2019). Analysis of the displacement at the toe of the landslide showed seasonal periods of movement with varying average velocity. Generally, the CET showed patterns of leveling out during dry periods, followed by sharp increases in displacement that coincided with rainfall, and finally a steady, near-continuous movement (advancement of the toe) during saturated or near-saturated conditions.

Field-derived SWCCs were developed in order to analyze shear strength and model suction stress. Slope location, soil type, and soil depths control the magnitudes of volumetric water content and water potential, and their response to rainfall. The modeled SWCCs for each landslide were different, meaning that the shapes of the curves derived for each landslide and associated slope location are a function of soil type, grain size, and soil-moisture behavior. The same parameters needed for field-based SWCCs were used in an extended Mohr-Coulomb failure criterion that calculated shear strength. A nonlinear shear-strength equation was used to determine the values of unsaturated soil parameters, calculating shear strength from saturated to residual soil conditions. Shear-strength values ranged from approximately 10 kPa to more than 250 kPa.

In addition to developing the SWCCs, we calculated suction stress and constructed models for soils at the Roberts Bend landslide. The nonlinear curves can be used to estimate permeability, water storage, and shear-strength functions. At the 70-cm-deep midslope location, the curve can clearly be divided into moisture regimes of transient water behavior, from saturated to dry. The transition zone is defined by the range of in-situ measurements of suction stress ranging from 200 kPa

to approximately 7 kPa. As with the SWCCs, the shape of the curve changes in this zone depends on the soil location and soil type.

Field and laboratory methods that focus on soil-water relationships have practical applications, such as investigating landslide occurrence and slope stability. Developing SWCCs and SSCCs is common practice in geotechnical engineering analysis of unsaturated-soil mechanics. Analyzing suction stress over time and correlating it with rainfall can be a proxy for changes in effective stress in a hillslope soil during wetting and drying.

Monitoring soil-moisture conditions, rainfall, and slope movement is the foundation for addressing various approaches to landslide susceptibility. A multidisciplinary field-monitoring approach that connects geologic processes and geotechnical parameters is important for broad landslide investigations, susceptibility modeling, or site-specific slope-stability assessment.

Acknowledgments

We would like to thank the Kentucky Geological Survey for financial and logistical support, especially Junfeng Zhu and Steve Webb of the KGS Water Resources Section. Terracon Consultants Inc. also provided financial support, as well as collaboration on geotechnical aspects of the project, through the Terracon Foundation. Many colleagues provided field and technical assistance: faculty, staff, and graduate students in the University of Kentucky Department of Earth and Environmental Sciences (special thanks to Peter Idstein, academic lab coordinator); Francis Ashland of the U.S. Geological Survey Landslide Hazards Program, whose advice about landslide monitoring and field instrumentation was invaluable and whose funding allowed for purchase of field instruments; and Glynn Beck and Junfeng Zhu of the KGS Water Resources Section, whose technical reviews improved the content and clarity of the report.

References Cited

Abramson, L.W., Lee, T.S., Sharma, S., and Boyce, G.M., 2002, Slope stability and stabilization methods [2d ed.]: New York, Wiley, 712 p.

Baum, R.L., Godt, J.W., and Savage, W.Z., 2010, Estimating the timing and location of shallow rainfall-induced landslides using a model for transient, unsaturated infiltration: Journal of Geophysical Research, v. 115, F03013, 26 p., doi.org/10.1029/2009JF001321.

Bittelli, M., Valentino, R., Salvatorelli, F., and Rossi Pisa, P., 2012, Monitoring soil-water and displacement conditions leading to landslide occurrence in partially saturated clays: Geomorphology, v. 173-174, p. 161–173, doi.org/10.1016/j.geomorph.2012.06.006.

Bordoni, M., Bittelli, M., Valentino, R., Chersich, S., and Meisina, C., 2017, Improving the estimation of complete field soil water characteristic curves through field monitoring data: Journal of Hydrology, v. 552, p. 283–305, doi:10.1016/j.hydrol.2017.07.004.

Budhu, M., 2007, Soil mechanics and foundations [2d ed.]: New York, Wiley, 634 p.

Campbell Scientific Inc., 2014, Instruction manual: CS650 and CS655 water content reflectometers: Campbell Scientific Inc., 36 p. plus 4 appendices.

Chen, P., Mirus, B., Lu, N., and Godt, J.W., 2017, Effect of hydraulic hysteresis on stability of infinite slopes under steady infiltration: Journal of Geotechnical and Geoenvironmental Engineering, v. 143, issue 9, p. 1–10, doi.org/10.1061/(ASCE)GT.1943-5606.0001724.

Coe, J.A., Ellis, W.L., Godt, J.W., Savage, W.Z., Savage, J.E., Michael, J.A., Kibler, J.D., Powers, P.S., Lidke, D.J., and Debray, S.P., 2003, Seasonal movement of the Slumgullion landslide as determined from Global Positioning System surveys and field instrumentation, July 1998–March 2002: Engineering Geology, v. 68, issues 1-2, p. 67–101, doi.org/10.1016/S0013-7952(02)00199-0.

Crawford, M.M., 2012, Using LiDAR to map landslides in Kenton and Campbell Counties, Kentucky: Kentucky Geological Survey, ser. 12, Report of Investigations 24, 12 p., doi.org/10.13023/kgs.ri24.12.

Crawford, M.M., 2018, Hydrologic monitoring and 2-D electrical resistivity imaging for joint geophysical and geotechnical characterization of shallow colluvial landslides: Lexington, University of Kentucky, doctoral dissertation, 153 p., doi.org/10.13023/etd.2018.393.

Crawford, M.M., and Bryson L.S., 2018, Assessment of active landslides using field electrical measurements: Engineering Geology, v. 233, p. 146–159, doi.org/10.1016/j.enggeo.2017.11.012.

Crawford, M.M., Bryson, L.S., Woolery, E.W., and Wang, Z., 2018, Using 2-D electrical resistivity imaging for joint geophysical and geotechnical characterization of shallow landslides: Journal of Applied Geophysics, v. 157, p. 37–46, doi:10.1016/j.jappgeo.2018.06.009.

Crawford, M.M., Bryson, L.S., Woolery, E.W., and Wang, Z., 2019, Long-term monitoring using soil-water relationships and electrical data to estimate suction stress: Engineering Geology, v. 251, p. 146–157.

Cruden, D.M., and Varnes, D.J., 1996, Landslide types and processes, *in* Turner, A.K., and Schuster, R.L., eds., Landslides: Investigation and mitigation: National Research Council, Transportation Research Board, Special Report 247, p. 278–316.

Czikowsky, M.J., and Fitzjarrald, D.R., 2004, Evidence of seasonal changes in evapotranspiration in eastern U.S. hydrological records: Journal of Hydrometeorology, v. 5, p. 974–988, doi.org/10.1175/1525-7541(2004)005<0974:EOSCIE>2.0.CO;2.

Das, B.M., 2010, Principles of geotechnical engineering [7th ed.]: Stamford, Conn., Cengage Learning, 666 p.

Decagon Devices Inc., 2017, MPS-2 & MPS-6 dielectric water potential sensors: Operator's manual: Decagon Devices Inc., 30 p.

Dong, Y., and Lu, N., 2017, Measurement of suction-stress characteristic curve under drying and wetting conditions: Geotechnical Testing Journal, v. 40, no. 1, p. 107–121, doi:10.1520/GTJ20160058.

Fleming, R.W., and Johnson, A.M., 1994, Landslides in colluvium: U.S. Geological Survey Bulletin 2059-B, 24 p.

Fredlund, D.G., Sheng, D., and Zhao, J., 2011, Estimation of soil suction from the soil-water characteristic curve: Canadian Geotechnical Journal, v. 48, no. 2, p. 186–198, doi:10.1139/T10-060.

Fredlund, D.G., and Xing, A., 1994, Equations for the soil-water characteristic curve: Canadian Geotechnical Journal, v. 31, no. 4, p. 521–532, doi.org/10.1139/t94-061.

Godt, J.W., Baskak, S., Lu, N., and Baum, R.L., 2012, Stability of infinite slopes under transient partially saturated seepage conditions: Water Resources Research, v. 48, no. 5, p. 1–14, doi:10.1029/2011WR011408.

Godt, J.W., Baum, R.L., and Lu, N., 2009, Landsliding in partially saturated materials: Geophysical Research Letters, v. 36, no. 2, p. 1–5, doi:10.1029/2008GL035996.

Guan, G.S., Rahardjo, H., and Leong, E.C., 2010, Shear strength equations for unsaturated soil under drying and wetting: Journal of Geotechnical and Geoenvironmental Engineering, v. 136, no. 4, p. 594–606, doi:10.1061/(ASCE)GT.1943-5606.0000261.

Lu, N., 2008, Is matric suction a stress variable: Journal of Geotechnical and Geoenvironmental Engineering, v. 134, no. 7, p. 899–905, doi:10.1061/(ASCE)1090-0241(2008)134:7(899).

Lu, N., and Godt, J.W., 2013, Hillslope hydrology and stability: New York, Cambridge University Press, 437 p.

Lu, N., Godt, J.W., and Wu, D.T., 2010, A closed form equation for effective stress in unsaturated soil: Water Resources Research, v. 46, no. 5, 14 p., doi:10.1029/2009WR008646.

Lu, N., Kaya, M., and Godt, J.W., 2014, Interrelations among the soil-water retention, hydraulic conductivity, and suction-stress characteristic curves: Journal of Geotechnical and Geoenvironmental Engineering, v. 140, no. 5, 04044007, doi.org/10.1061/(ASCE)GT.1943-5606.0001085.

Lu, N., and Likos, W.J., 2004, Unsaturated soil mechanics: Hoboken, N.J., Wiley, 556 p.

Lu, N., and Likos, W.J., 2006, Suction stress characteristic curve for unsaturated soil: Journal of Geotechnical and Geoenvironmental Engineering, v. 132, no. 2, p. 131–142, doi:10.1061/(ASCE)1090-0241(2006)132:2(131).

Luft, S.J., 1969, Geologic map of the Independence quadrangle, Kenton and Boone Counties, Kentucky: U.S. Geological Survey Geologic Quadrangle Map GQ-785, scale 1:24,000.

Morris, R.H., 1965, Geologic map of the Charters quadrangle, Kentucky: U.S. Geological Survey Geologic Quadrangle Map GQ-293, scale 1:24,000.

Oh, S., and Lu, N., 2015, Slope stability analysis under unsaturated conditions: Case studies of rainfall-induced failure of cut slopes: Engineering Geology, v. 184, p. 96–103, doi.org/10.1016/j.enggeo.2014.11.007.

Potter, P.E., 2007, Exploring the geology of the Cincinnati/northern Kentucky region [2d rev. ed.]: Kentucky Geological Survey, ser. 12, Special Publication 8, 128 p.

Rhoades, J.D., Raats, P.A.C., and Prather, R.J., 1976, Effects of liquid-phase electrical conductivity, water content, and surface conductivity on bulk soil electrical conductivity: Soil Science Society of America Journal, v. 40, no. 5, p. 651–653, doi:10.2136/ssaj1976.03615995004000050017x.

Smith, J.B., Godt, J.W., Baum, R.L., Coe, J.A., Burns, W.J., Lu, N., Morse, M.M., Sener-Kaya, B., and Kaya, M., 2013, Hydrologic monitoring of a landslide-prone hillslope in the Elliot State Forest, Southern Coast Range, Oregon, 2009–2012: U.S. Geological Survey Open-File Report 2013-1283, 61 p.

Taylor, A.R., Lewis, R.Q., Sr., and Smith, J.H., 1975, Geologic map of the Burnside quadrangle, south-central Kentucky: U.S. Geological Survey Geologic Quadrangle Map GQ-1253, scale 1:24,000.

Topp, G.C., Davis, J.L., and Annan, A.P., 1980, Electromagnetic determination of soil water content: Measurements in coaxial transmission lines: Water Resources Research, v.16, no.3, p.574–582, doi.org/10.1029/WR016i003p00574.

Turner, A.K., 1996, Colluvium and talus, *in* Turner, A.K., and Schuster, R.L., eds., Landslides: Investigation and mitigation: National Research Council, Transportation Research Board, Special Report 247, p.525–554.

Vanapalli, S.K., Fredlund, D.G., Pufahl, D.E., and Clifton, A.W., 1996, Model for the prediction of shear strength with respect to soil suction: Canadian Geotechnical Journal, v.33, no.3, p.379–392, doi:10.1139/t96-060.

Van Genuchten, M.T., 1980, A closed-form equation for predicting the hydraulic conductivity of unsaturated soils: Soil Science Society of America Journal, v.44, no.5, p.892–898, doi:10.2136/sssaj1980.03615995004400050002x.